Astron. Astrophys. Suppl. Ser. 103, 157-182 (1994)

High-frequency radio continuum observations of radio galaxies with low and intermediate luminosity.

II. Sources with sizes 4' to 5'

K.-H. Mack¹, L. Gregorini^{2,3}, P. Parma² and U. Klein⁴

- ¹ Max-Planck-Institut für Radioastronomie, Auf dem Hügel 69, D-53121 Bonn, Germany
- ² Istituto di Radioastronomia, Via Irnerio 46, 40126 Bologna, Italy
- 3 Dipartimento di Fisica, Universitá di Bologna, Via Irnerio 46, 40126 Bologna, Italy
- ⁴ Radioastronomisches Institut der Universität, Auf dem Hügel 71, D-53121 Bonn, Germany

Received April 26; accepted June 16, 1993

Abstract. — We have mapped 17 low and intermediate luminosity radio galaxies with angular sizes between 4' and 5' using the Effelsberg 100-m telescope. These sources were selected from the B2 and 4C catalogue in an on-going project to study the high-frequency radio continuum and polarization characteristics of such sources. The integrated radio spectra between 408 MHz and 10.6 GHz are found to resemble those of strong 3C sources, the average spectral index being $\alpha = -0.69 \pm 0.02 \ (S_{\nu} \propto \nu^{\alpha})$. In most of the sources, high degrees of linear polarization are seen, indicating that the magnetic fields in these sources are ordered over large scales. The orientation of the magnetic fields exhibits a clear trend of two preferential direction configurations, viz. parallel and perpendicular to the sources' axes or, equivalently, their jets. Furthermore, the trend for parallel fields to prevail in sources with brighter cores is indicated in our data, despite the small sample of sources involved in this study.

Key words: radio continuum: galaxies — polarization — magnetic fields

1. Introduction

We have embarked on a study of low and intermediate luminosity radio galaxies at 10.6 GHz using the Effelsberg 100-m telescope (Gregorini et al. 1992, hereafter Paper I) with the aim to study their radio spectra, the spectral index distributions across these sources, their rotation measures (RMs) and their overall magnetic field structures. In Paper I we reported observations of ten sources with angular extents $\geq 4'$, along with a discussion of the high-frequency properties. Here we extend this study to sources with angular dimensions 4'-5'. A total of 17 sources has been mapped at 10.6 GHz.

In Sect. 2 the observational technique and data reduction procedure are briefly outlined. In Sect. 3 we present the results, along with some discussion of the individual sources, while in Sect. 4 we summarize the results. The distributions of the spectral indices and the RM, depolarization and magnetic field characteristics will be presented in forthcoming papers.

2. Observations and data analysis

For the present study a total of 16 sources has been culled from those objects that have previously been observed with high angular resolution using the WSRT and the VLA (see Fanti et al. 1987; Gregorini et al. 1988; and references therein). These sources are still large enough to be studied in some detail with the 69" beam of the 100-m telescope at 10.6 GHz. In addition, a deep map of the source 0828+32 has been obtained with the aim to trace the weak emission from its 'old' lobes which had not been detected in our previous measurements (Paper I). For a detailed description of the observing and data reduction technique we refer the reader to Paper I, in which we have detailed the basic operation of the new 10.6 GHz multibeam receiver system installed in the secondary focus of the 100-m telescope, along with the mapping technique of extended sources (Emerson et al. 1979). The final Stokes I maps have in addition been CLEANed using the Högbom (1974) algorithm. To this end, a high-dynamic range $(\gtrsim 34 \text{ dB})$ map of 3C84, 10' in size, was used as the dirty beam. The observations have been carried out between

Table 1. List of sources and map parameters

Source	Field ce	entre	Map size	Number of		of	rms noise	
	$\mathrm{RA_{50}}$	$\mathrm{DEC_{50}}$		coverages		[mJy/b.a.]		
	[h:m:s]	[°:':'']	$[' \times ']$	I	U	Q	I	$ m I_p$
0136+39A	01:36:33.7	39:41:53	10.3×10.3	11	11	11	0.8	0.5
0204+29	02:04:08.8	29:16:31	7.7×7.7	11	11	11	0.8	0.5
0828+32	08:28:20.6	32:29:37	16.7 imes 16.7	39	40	40	0.6	0.3
0836 + 29	08:36:13.5	29:01:16	9.3×9.3	11	11	11	0.8	0.5
1102+30	11:02:39.7	30:25:53	7.3×7.3	11	11	11	0.6	0.5
1141+37	11:41:50.0	37:25:06	8.3×8.3	11	11	11	1.3	0.7
1243+26	12:43:54.6	26:43:39	8.3×8.3	11	11	11	0.6	0.5
1316+29	13:16:43.0	29:54:20	7.3×7.3	11	11	11	0.7	0.6
1339+26	13:39:35.0	26:38:10	6.7×6.7	5	5	5	0.8	0.6
1357+28	13:57:45.2	28:44:28	6.7×6.7	11	11	11	0.7	0.6
1422+26	14:22:26.5	26:51:02	6.3×6.3	11	11	11	0.6	0.5
1441+26	14:41:53.0	26:13:51	7.3×7.3	11	11	11	0.6	0.5
1455+28	14:55:45.5	28:44:16	6.7×6.7	11	10	11	0.7	0.5
1528+29	15:28:05.9	29:10:43	7.3×7.3	13	13	13	0.6	0.5
1637+29	16:37:22.2	29:56:47	8.0×8.0	14	14	14	0.7	0.5
1658+30A	16:58:45.1	30:12:32	8.0×8.0	11	11	11	0.6	0.5
2249+37	22:49:06.3	37:56:45	7.3×7.3	11	11	11	0.6	0.5

January 1990 and October 1991. Calibration, pointing and polarization performance of the system have been checked and achieved by frequently cross-scanning and mapping the point sources 3C48, 3C123, 3C138, 3C147, 3C286, 3C295, and NGC 7027. The adopted calibration scale is that of Baars et al. (1977), with the re-adjustment of this scale for some of these sources reported by Ott (1991) accounted for (see Paper I for more details).

In Table 1 the map parameters for each source are compiled. The map centres given there are not necessarily the positions of the galaxies (which can be found in Fanti et al. 1977; 1978 and Gregorini et al. 1988). The map sizes refer to the final maps presented here. As is evident in Table 1, the computed rms noise values do not always reflect the coverage of the sources, owing to varying weather conditions and hence imperfect cancellation of atmospheric noise.

3. Results

3.1. Radio maps at 10.6 GHz

In Figs. 1 through 17 we present the total and polarized intensity maps at 10.6 GHz of the sources investigated here. The vector represented in the polarized maps indicates the magnetic field orientation, i.e. the E-vector rotated by 90°. Table 2 contains the contour levels for each map. In what follows we briefly describe the main characteristics of each source, and compare them with observations at other frequencies.

3.1.1. 0136+39 (4C39.04)

A first detailed radio continuum study of this giant (1.3 Mpc) radio source was published by Hine (1979), who found a steepening of the spectrum from its outer ends towards the centre. In fact the spectrum of the central source is rather steep ($\alpha=-1.0$, according to Hine, 1979). Our 10.6 GHz map (Fig. 1a) shows the core to be just visible at this frequency. A Gaussian fit to the map in this area yields a flux density of 4 ± 1 mJy, implying a steepening of the spectrum to $\alpha=-1.7\pm 0.4!$ This spectrum suggests that the core is extended and may have a jet, although high-resolution interferometric observations reported so far detected a point source only (see Fomalont & Bridle, 1978; Katgert-Merkelijn et al. 1980; and Gregorini et al. 1988). VLBI observations of this peculiar central source are mandatory.

Figures 1a and b show that the magnetic field in 4C39.04 is parallel to the source axis essentially over its whole extent. Strong linear polarization is seen, with degrees of up to 60% at the outer edges of the lobes.

3.1.2. 0204+29 (4C29.06)

Figure 2 shows the maps of this double source. The source at $RA_{50} = 02^h04^m01.1^s$, $DEC_{50} = 29^\circ14'10''$ is a background object (Meurs & Unger 1991) although it shows considerable polarization. A strong asymmetry is visible in the polarized emission of the lobes. The eastern one is more strongly polarized and its magnetic field is exactly parallel to the source axis. Although the orientation of the magnetic field in the western lobe is essentially par-

allel to the source axis, too, its alignment is less uniform. High-resolution radio continuum maps (Gregorini et al. 1988) show a more diffuse structure in this lobe, with no indications of a jet.

3.1.3.0828+32

This source was already observed at 10.6 GHz by Gregorini et al. (1992). We have reobserved it as the previous map was not large enough to show the full extent of the secondary lobe system (Parma et al. 1985) which can be traced even at this high radio frequency. We have therefore combined the previous map and the new one, with weights proportional to the inverse square of the rms noise.

Figure 3a clearly shows the secondary, and presumably old, lobe system, which at lower frequencies and higher resolution looks rather detached from the presumably young lobes. Again, an asymmetry is seen in the two main lobes: the western one is brighter in total intensity, while the eastern one is more strongly polarized (see Fig. 3b). The whole source is strongly polarized, with degrees of up to 40%. Surprisingly, the highest degrees of polarization are found in the old lobe system, with the highest values occurring in the southern one. The projected orientation of the magnetic field is perpendicular to the source axis in the young lobes, while in the old lobes it appears to follow these rather precisely.

3.1.4. 0836+29

This source is associated with the brightest galaxy in the cluster A690 (de Ruiter et al. 1986). According to Valentijn (1979) it is a wide-angle tail source. The dominating component in our map (Fig. 4a) is the central source, which has a flat spectrum ($\alpha = -0.17$, $S_{\nu} \sim \nu^{\alpha}$). The most salient feature in our polarization map (Fig. 4b) is the bright polarized component south of the nucleus where the radio structure exhibits a sharp bend towards the north-west. The strong polarization in this region is certainly not accidental and may be related to a compression of the magnetic field at the location of the kink. This is corroborated by the fact that the observed magnetic field is oriented perpendicular to the source axis at this position (Fig. 4b).

3.1.5.1102+30

This double source (Fanti et al. 1977) is not fully resolved by our 69" beam (Fig. 5a), but nevertheless shows a strong asymmetry in the map of linear polarization at 10.6 GHz (Fig. 5b). The eastern part of the source is strongly polarized, while the western one shows much less linear polarization.

Astronomy and Astrophysics, Vol. 103, N° 1, January 1994. — $6\,$

3.1.6. 1141+37 (4C37.32)

The most likely host galaxy of this radio source lies in a chain of 4 galaxies. A giant radio halo was reported by Malumyan (1984); our total power map at 10.6 GHz (Fig. 6a) shows protrusions which may also be connected with it. The most pronounced one is seen to emerge from the north-eastern lobe towards the north, while there is only a marginal indication of such a feature to emerge from the south-eastern lobe towards the south. Both of these are obviously related to the structures seen to turn away from the lobes at higher resolution by de Ruiter et al. (1986), who used the VLA at $\lambda 20$ cm in its Cconfiguration. The map of linear polarization (Fig. 6b) shows that the magnetic field orientations are different in the two lobes, with a perpendicular field in the northeastern lobe and a parallel field in the other one. The degrees of polarization are relatively low, with typical values of about 10% across the source. Given that this is not caused by Faraday depolarization, it means that the magnetic field is rather tangled, which could be related to the complex structure of the source on the whole.

3.1.7. 1243+26

The host galaxy of this source is located in the galaxy cluster A1609. There are two optically visible galaxies lying within the radio contours. The corresponding positions marked "x" in Fig. 7a are taken from de Ruiter et al. (1986). We may face a situation of interacting galaxies producing a complex radio structure (Valentijn 1979). Our map of linear polarization (Fig. 7b) uncovers strong polarization at the position of the sharp bend of the northern jet seen in the high-resolution maps of de Ruiter et al. (1986) and Owen et al. (1992), with degrees of $\sim 20\%$. The polarized brightness in the southern part of the source is somewhat less, probably as a result of beam depolarization caused by the complex magnetic field structure there.

3.1.8.1316+29

The s-shaped structure of this source which is visible at high resolution (de Ruiter et al. 1986; Fanti et al. 1987) has been smeared out by our 69" beam (Fig. 8a). The mean orientation of the magnetic field is perpendicular to the source axis. The typical degrees of polarization of $\sim 15\% - 20\%$ indicate significant beam depolarization (see Fig. 8b). This is explicable if the field follows the complex structure seen on small scales.

3.1.9.1339+26

Due to the limited coverage of this source (see Table 1) the 10.6 GHz maps (Fig. 9) show only the brightest feature, which is the head of this head-tail source, located in the cluster A1775. The tail seen at lower frequencies (de Ruiter et al. 1986) is below the noise in our map.

Table 2. Contour levels of the maps (mJy/b.a.)

Source	Figure	Contour levels	Figure	Contour levels
		Total intensity		Polarization
0136+39A	1a	1.5,3,5,7,10,15,20,25	1b	1,1.5,2,2.5,3,3.5
0204+29	2a	2,4,6,8,10,15,20,30,40,60,80,100,120,140	2b	1,2,3,4,5,6,7,8,9,10,11,12
0828+32	3a	1,2,4,7,10,15,20,30,40,50,60,70,80,90,100,110	3b	0.5,1,2,4,6,8,10,12,14,16,18,20
0836+29	4a	2,4,7,10,15,20,30,40,60,80,100,120,140	4b	1,2,4,6,8,10
1102+30	5a	1,2,4,6,8,10,15,20,25,30,35,40	5b	1, 1.5, 2, 2.5, 3, 3.5, 4, 4.5, 5, 5.5
1141+37	6a	3,5,7,11,15,20,30,40,60,80,100,120,140,160	6b	1,2,3,4,5,6
1243+26	7a	1.5,3,5,7,10,15,20,25,30	7b	1, 1.5, 2, 2.5, 3, 3.5
1316+29	8a	2,4,7,10,15,20,30,40,60,90	8b	1,2,4,6,8,10,12
1339+26	9a	2,4,6,8,10,15,20,25,30,35	9b	1.5, 2, 2.5
1357+28	10a	2,4,6,8,10,15,20,25,30	10b	0.75, 1, 1.25
1422+26	11a	1.5, 3, 6, 10, 15, 20, 30, 40, 50, 60, 70, 80, 90	11b	1,2,4,6,8,10
1441+26	12a	1.5,3,5,7,10,13,15	12b	1,1.5,2
1455+28	13a	1, 2, 4, 7, 10, 15, 20, 30, 40, 50, 60	13b	1,2,3,4
1528+29	14a	1.5,3,5,7,9,11	14b	1,1.5
1637+29	15a	2,4,6,8,10,15,20,25,30	15b	1, 1.5, 2, 2.5, 3, 3.5, 4
1658+30A	16a	1, 2, 4, 7, 10, 15, 20, 30, 40, 60, 80, 100, 120	16b	1,2,3,4,5,6,7
2249+37	17a	2,4,7,10,15,20,30,40,50,60	17b	1,2,3,4,5

3.1.10.1357+28

This radio source (de Ruiter et al. 1986) is not resolved at 10.6 GHz (Fig. 10a). The source is characterized by low degrees of linear polarization, which hardly reach 10%. This may be due to the beaming depolarization.

3.1.11.1422+26

The double structure of this source (Ekers et al. 1981) is smoothed to an elongated structure in our total power map (Fig. 11a), but is clearly discernable in the map of linear polarization (Fig. 11b). The degrees of polarization are fairly high, with values of up to $\sim 20\%$ near the outer lobe edges. The magnetic field is oriented perpendicular to the source axis throughout. The polarization angles at 1415 and 2700 MHz (Ekers et al. 1981; Parma & Weiler 1981) indicate little Faraday rotation for this source.

3.1.12.1441+26

An asymmetry in the total luminosity of the two lobes is present in our 10.6 GHz map: the eastern lobe is almost twice as bright as the western one, as Fig. 12a shows. The degrees of polarization are modest, with values between 15% and 20% (Fig. 12b), probably again owing to the complex source structure seen at higher resolution (Fanti et al. 1987). The eastern lobe is more strongly polarized than the western one. The magnetic field orientation is different in the two lobes, viz. parallel to the source axis in the eastern one, and almost perpendicular in the west.

3.1.13.1455+28

This edge-brightened source has a rather symmetric appearance at 10.6 GHz (Fig. 13a). Low degrees of polarization (<10%) may be connected with the lateral extensions of the source seen at high resolution (de Ruiter et al. 1986; Fanti et al. 1987). The overall orientation of the magnetic field is parallel to the source axis except near the centre, where the field is seen to turn off (Fig. 13b). This, too, may be related to the lateral protrusions.

3.1.14. 1528+29

This source has a more asymmetric brightness distribution at 10.6 GHz (Fig. 14a) as compared to its appearance at lower frequencies (conf. de Ruiter et al. 1986). Fig. 14a gives the impression of an edge-darkened source, while at $\lambda 20$ cm it looks more like edge-brightened. This indicates a rapid steepening of the spectrum towards the outer edges of the lobes. The distribution of the linear polarization is asymmetric, too. The western lobe is strongly polarized (> 30%), while the eastern one exhibits much less polarization (Fig. 14b). The magnetic field is essentially perpendicular to the source structure.

3.1.15.1637+29

This peculiar source is a head-tail source associated with a poor group of galaxies (de Ruiter et al. 1986). The western component (denoted "b" by Parma et al. 1985) is the dominant feature, but also component "a" is still visible at 10.6 GHz (Fig. 15a). Strong polarization is found in the bright western component, with typical degrees

Table 3. Integral	quantities of	the sources	at 10.55	GHz
-------------------	---------------	-------------	----------	-----

						log		
Source	z	D^*	$S_{ m tot}$		χ	$P(10.55\mathrm{GHz})$	lpha	RM
		[Mpc]	[mJy]	[%]	[°]	$[\mathrm{WHz^{-1}}]$		$[\operatorname{rad} m^{-2}]$
0136+39A	0.2107	522	115± 7	13.3 ± 3.4	129 ± 7	24.58	-0.89 ± 0.01	
0204+29	0.1090	295	504 ± 11	5.3 ± 0.9	144 ± 5	24.72	-0.58 ± 0.05	_
0828+32	0.0507	145	528 ± 11	7.8 ± 0.5	74 ± 1	24.12	-0.66 ± 0.02	27± 3
0836+29	0.0790	220	299 ± 10	3.7 ± 2.1	9 ± 25	24.24	-0.42 ± 0.06	32±16
1102+30	0.0720	201	100 ± 5	12.2 ± 3.5	69 ± 8	23.68	-0.68 ± 0.04	13± 3
1141+37	0.1145	308	$442 {\pm} 14$	$1.4 {\pm} 1.4$	142 ± 23	24.70	-0.76 ± 0.06	-17 ± 13
1243+26	0.0891	245	99 ± 4	9.0 ± 2.4	32 ± 5	23.85	-0.67 ± 0.03	14± 6
1316+29	0.0728	204	301 ± 7	9.7 ± 1.7	99 ± 4	24.17	-0.66 ± 0.02	2± 2
1339+26	0.0757	211	51 ± 4	2.0 ± 7.2	102 ± 93	23.43	-0.98 ± 0.05	
1357+28	0.0629	178	74 ± 4	2.9 ± 3.8	43 ± 57	23.45	-0.68 ± 0.04	14±24
1422+26	0.0370	107	212 ± 5	$9.4{\pm}1.4$	108 ± 5	23.46	-0.67 ± 0.04	3± 4
1441+26	0.0621	175	42 ± 5	$6.5 {\pm} 9.0$	153 ± 36	23.19	-0.87 ± 0.04	15±15
1455+28	0.1411	371	187 ± 5	$3.4 {\pm} 1.2$	133 ± 10	24.49	-0.68 ± 0.04	13± 8
1528+29	0.0843	233	42 ± 5	16.0 ± 8.7	92 ± 20	23.43	-0.77 ± 0.08	0± 9
1637+29	0.0875	241	100 ± 11	11.9 ± 6.7	160 ± 16	23.84	-0.55 ± 0.04	
1658+30A	0.0351	102	252 ± 8	$5.4 {\pm} 0.7$	66 ± 3	23.49	-0.45 ± 0.05	15± 4
2249+37			242± 6	4.5±1.2	102±10		-0.61 ± 0.02	

^{*} $H_0 = 100 \,\mathrm{km/s/Mpc}$ and $q_0 = 1$ assumed.

of ~20% (see Fig. 15b). This polarized emission must be associated with the brightest western tail resolved in the radio-optical study of de Ruiter et. al. (1988). No significant polarization is seen though in the eastern component, in line with the findings of Parma et al. (1985). This is obviously caused by beam depolarization in the strongly bending tails of the source which are shaped by the strong gravitational interaction of the host and the companion galaxy (de Ruiter et al. 1988). The magnetic field is oriented perpendicular to the jets.

3.1.16. 1658+30A

As in case of 1422+26 the core-lobe structure of this "fat double" source (Feretti et al. 1983; de Ruiter et al. 1986) is smeared out by our beam at 10.6 GHz (Fig. 16a). In the map of linear polarization a double structure is visible though (Fig. 16b). The source to the north-west is not related to this radio galaxy. Strong linear polarization is found near the lobes' edges, with values of 40%-50%. The magnetic field orientation is essentially perpendicular to the source axis.

3.1.17. 2249+37 (4C37.66)

This source, which shows a complex structure, is associated with a cluster galaxy (Katgert-Merkelijn et al. 1980). The detailed structure is smeared out in our total power map (Fig. 17a). In spite of the complex structure we find strong polarization at 10.6 GHz (Fig. 17b), with degrees of up to $\sim 20\%$. The magnetic field structure is rather

complicated, too. Comparison with the 1415 MHz map of Katgert-Merkelijn et al. shows that in fact it follows the different source components quite precisely.

3.2. Integral source properties

We have also derived integral properties of the sources (10.6 GHz flux densities and monochromatic radio luminosities, spectral indices, mean degrees of polarization, mean polarization angles), and have collected them in Table 3. The integrated flux densities were derived by integrating the maps in elliptical rings, with the ellipses adapted to the source shapes and positions angles. Spectral indices were also derived for source components wherever the angular resolution was sufficient to do so. To this end, the component flux densities at 10.6 GHz were integrated in rectangular areas and compared with comparable data in the literature. A more thorough spectral index analysis via point-to-point comparisons of maps at two frequencies will follow in a forthcoming paper.

A comparison with data at lower frequencies also allowed us to calculate mean RMs of the sources as well as RMs in different components of the objects. To this end, we have computed mean Stokes I, U, and Q brightnesses in the same regions in which other authors determined mean polarization degrees and angles. Those data have been taken from the work of Ekers et al. (1981), Parma & Weiler (1981), and de Ruiter et al. (1986). The resulting degrees of polarization and polarization angles of the different source components at 10.6 GHz are compiled in Table 4, along with the deduced RMs.

Table 4. Total and component rotation measures of the sources

Source	Component	< α >	< p _{10.55} >	X10.55	RM
}			[%]	[°]	$[\mathrm{rad}\mathrm{m}^{-2}]$
0136+39	E lobe		10.7 ± 2.7	130 ± 7	
	W lobe		14.7 ± 4.0	129 ± 7	
0204+29	E lobe		$7.6 {\pm} 0.7$	140 ± 3	_
	W lobe		3.8 ± 0.6	156 ± 5	_
0828+32	W lobe	-0.65 ± 0.02	13.3 ± 0.5	79 ± 1	27 ± 2
	E lobe	-0.66 ± 0.06	5.2 ± 0.4	52 ± 2	32 ± 2
	N old lobe	~ -0.93	_	-	
	S old lobe	~ -0.92		_	_
0836+29	N lobe	-0.84	7.5 ± 4.1	125 ± 13	-4 ± 8
	centre	-0.17			-21 ± 30
	S lobe	-0.69	17.7 ± 1.7	4 ± 4	20± 6
1102+30	W lobe	-0.59 ± 0.05	8.2 ± 3.3	67 ± 11	-
	centre		11.7 ± 1.8	76 ± 4	- 1
	E lobe	-0.90 ± 0.08	15.1 ± 3.9	70 ± 7	_
1141+37	N lobe	-0.76 ± 0.06	1.8 ± 1.0	68 ± 16	15± 9
	S lobe	-0.75 ± 0.08	3.9 ± 1.3	135 ± 8	-6 ± 6
1243+26	N lobe	-0.47	16.1 ± 5.3	42 ± 9	19± 4
	centre	-0.63	10.8 ± 2.1	32 ± 6	0± 2
	S lobe	-0.67	5.1 ± 2.8	19 ± 16	_
1316+29	E lobe	-0.79	11.1 ± 2.0	103 ± 4	2± 2
	centre	+0.06	10.4 ± 1.1	95 ± 2	0± 2
	W lobe	-0.76	7.8 ± 2.0	98 ± 6	1± 3
1339+26	head	-0.80			
1357+28	N lobe		$3.6 {\pm} 5.4$	53 ± 44	
	S lobe		4.3 ± 5.7	161 ± 36	
1422+26	E lobe		6.1 ± 1.3	105 ± 7	_
	W lobe		12.4 ± 1.3	111 ± 3	_
1441 + 26	W lobe	-1.04 ± 0.10	$9.5 \pm 11.$	135 ± 25	7±11
	E lobe	-0.86 ± 0.05	13.3 ± 5.8	157 ± 12	17± 5
1455 + 28	S lobe	-0.71 ± 0.06	$4.9{\pm}1.5$	140 ± 9	11± 6
	N lobe	-0.73 ± 0.03	1.3 ± 1.6	120 ± 36	15±18
1528+29	W lobe	-0.87	20.0 ± 7.6	103 ± 10	5± 5
	centre		9.1 ± 6.5	69 ± 18	_
	E lobe	-1.05	$12.7 \pm 11.$	58 ± 27	7±11
1658+30	E lobe		8.3 ± 1.4	85 ± 4	
	centre		3.9 ± 0.6	52 ± 5	
	W lobe		$6.9 {\pm} 1.2$	48 ± 6	

The spectral indices in Table 3 are average values over the whole frequency range over which the sources have been studied so far (i.e. typically from 408 MHz to $10.6~\mathrm{GHz}$). Analysis of the individual spectra shows that most of them are straight up to $10.6~\mathrm{GHz}$, except for a few which have breaks near $\sim 1~\mathrm{GHz}$, with changes of the spectral index of between $0.2~\mathrm{and}~0.4$. Most of the sources which show a high-frequency steepening in their spectra have their magnetic fields predominantly oriented along the source axis. Whether this is accidental or not cannot be decided at this stage. The integral spectral indices, together with those from Paper I (except 0924+30), have

been compiled in the histogram of Fig. 18. The resulting mean value is $\alpha = -0.69$, with a scatter of 0.14. This is consistent with the value of $\alpha = -0.75$ (dispersion of 0.29) found for the B2 sample in the range 408 MHz to 1415 MHz (de Ruiter et al. 1990). Our preliminary investigation of the spectra of the outer lobes do not show any pronounced differences except in 1102+30, in which the western (less polarized) lobe has a spectrum which is flatter by about 0.3 than the eastern one (see Table 4).

Except for a few sources, low-frequency polarization data exist for the objects studied here. We have made an attempt to derive rotation measures for the sources and their individual components. Most of the low-frequency data are based on measurements with the VLA at $\lambda 20$ cm (see Capetti et al. (1993) for the B2 sources). Comparing the polarization angles between $\lambda 20$ cm and $\lambda 2.8$ cm, there is an ambiguity of $n*73.3\,\mathrm{rad}\,\mathrm{m}^{-2}$, where n is an integer, since

$$RM = \frac{\chi_1 - \chi_2}{\lambda_1^2 - \lambda_2^2} + \frac{n \cdot \pi}{\lambda_1^2 - \lambda_2^2} \ , \ n = 0, \pm 1, \pm 2, \dots$$

Using minimum energy arguments and inferring thermal electron densities of $n_{\rm e} \sim 3~10^{-3}~{\rm cm}^{-3}$ (see e.g. Morganti et al. 1988), we have tried to remove the ambiguities by calculating expected rotation measures. A uniform component of the magnetic field was estimated using the observed degrees of polarization and assuming that beam depolarization is the only mechanism diminishing the theoretical fractional polarization. The resulting rotation measures (with the lowest possible absolute values) are assembled in Table 3 and displayed in the histogram of Fig. 19. These values are moderate, and hardly exceed 20–30 rad m⁻². Those of the source components are given in Table 4. In view of the uncertainties there is no significant difference in the rotation measures of the different lobes.

Our measurements, though giving only moderate spatial resolution, provide us with a fairly fast technique of measuring mean magnetic field orientations across the sources (see Sect. 3.1). Here we utilize this in order to compute the relative orientation of the magnetic field and the jet in each source. To this end, we have determined the orientations of the jets by inspecting the high-resolution maps published by de Ruiter et al. (1986), Gregorini et al. (1988), and Ekers et al. (1981). These were compared with the mean magnetic field orientations within the corresponding components (obtained from the polarization angles in Table 4, rotated by 90°). The resulting differences Φ of the jet and magnetic field orientations are displayed in the histogram in Fig. 20. Clearly, there is a region of avoidance around 45°. This means that the mean magnetic field is either perpendicular or parallel to the jet axes. This may be understood if the overall magnetic field has a helical structure. The projected magnetic field component then depends primarily on the pitch angle of the helix. A stretched helix produces a predominantly parallel field, while a tight one gives rise to the observation of a perpendicular field. We furthermore notice a marginal tendency for the magnetic field to be parallel to the jets for sources whose core luminosities at 5 GHz (Giovannini et al. 1988) exceed $\sim 10^{23} \, \mathrm{W \, Hz^{-1}}$. This is in line with what has been established for source samples covering larger ranges in luminosity (see e.g. Bridle 1982).

4. Summary and conclusions

A sample of 16 sources with angular sizes between 4′ and 5′ has been mapped at 10.6 GHz using the Effelsberg 100-m telescope. In addition, a deep map of the source 0828+32 has been obtained in order to search for high-frequency emission from the old lobes of this peculiar radio galaxy. Most of the sources exhibit straight total radio spectra up to 10.6 GHz; a steepening of the integral spectrum at higher frequencies is indicated only in a few cases. The distribution of spectral indices is similar to that of sources with intermediate and high radio luminosities, with a mean value of $\alpha = -0.69$.

In spite of our relatively low spatial resolution there is copious information especially in the maps of linear polarization. The observed degrees of polarization are generally low in sources with complex morphologies (evident in high-resolution WSRT and VLA maps), while in those with a simple (core/jet/lobe) structure we find high degrees of polarization, with values of up to 50% locally. The magnetic fields are seen to have two preferential orientations with respect to the sources' axes or jets, viz. either perpendicular or parallel. This is interpreted in terms of their presumed helical structure. The observed integrated rotation measures of the sources are rather low, with values hardly exceeding some 20 rad m⁻².

Where possible we have determined some properties of the individual lobes of the sources. At this stage, there exist no significant asymmetries in the spectral indices and rotation measures of different lobes. A more thorough investigation involving point-by-point comparisons is in progress and will be published elsewhere.

References

Baars J.W.M., Genzel R., Pauliny-Toth I.I.K., Witzel A. 1977, A&A 61, 99

Bridle A.H. 1982. In: Heeschen D.S., Wade C.M. eds. Proc.IAU Symp. 97, Extragalactic Radio Sources, Reidel,Dordrecht, p. 121

Capetti A., Morganti R., Parma P., Fanti R. 1993, A&AS, in press

de Ruiter H.R., Parma P., Fanti C., Fanti R. 1986, A&AS 65, 111

de Ruiter H.R., Parma P., Fanti R., Ekers R.D. 1988, ApJ 329, 225

de Ruiter H.R., Parma P., Fanti C., Fanti R. 1990, A&A 227, 351

Ekers R.D., Fanti R., Lari C., Parma P. 1981, A&A 101, 194

Emerson D.T., Klein U., Haslam C.G.T. 1979, A&A 76, 92

Fanti C., Fanti R., Gioia I.M. et al. 1977, A&AS 29, 279

Fanti R., Gioia I.M., Lari C., Ulrich M.H. 1978, A&AS 34, 341

Fanti C., Fanti R., de Ruiter H.R., Parma P. 1987, A&AS 69, 57

Feretti L., Giovannini G., Gregorini L., Parma P. 1983, A&A 126, 311

Fomalont E.B., Bridle A.H. 1978, AJ 83, 725

Giovannini G., Feretti L., Gregorini L., Parma P. 1988, A&A 199, 73

Gregorini L., Padrielli L., Parma P., Gilmore G. 1988, A&AS 74, 107

Gregorini L., Klein U., Parma P., Schlickeiser R., Wielebinski R. 1992, A&AS 94, 13 Hine R.G. 1979, MNRAS 189, 527 Högbom J.A. 1974, A&AS 15, 417

Katgert-Merkelijn J., Lari C., Padrielli L. 1980, A&AS 40, 91

Malumyan V.G. 1984, Sov. Astron. Lett. 10, 35 Meurs E.J.A., Unger S.W. 1991, A&A 252, 63

Morganti R., Fanti R., Gioia I.M. et al. 1988, A&A 189, 11

Ott M. 1991, Diploma thesis, University of Bonn Owen F.N., White R.A., Burns J.O. 1992, ApJS 80, 501 Parma P., Ekers R.D., Fanti R. 1985, A&AS 59, 511 Parma P., Weiler K.W. 1981, A&A 96, 412

Valentijn E.A. 1979, A&AS 38, 319

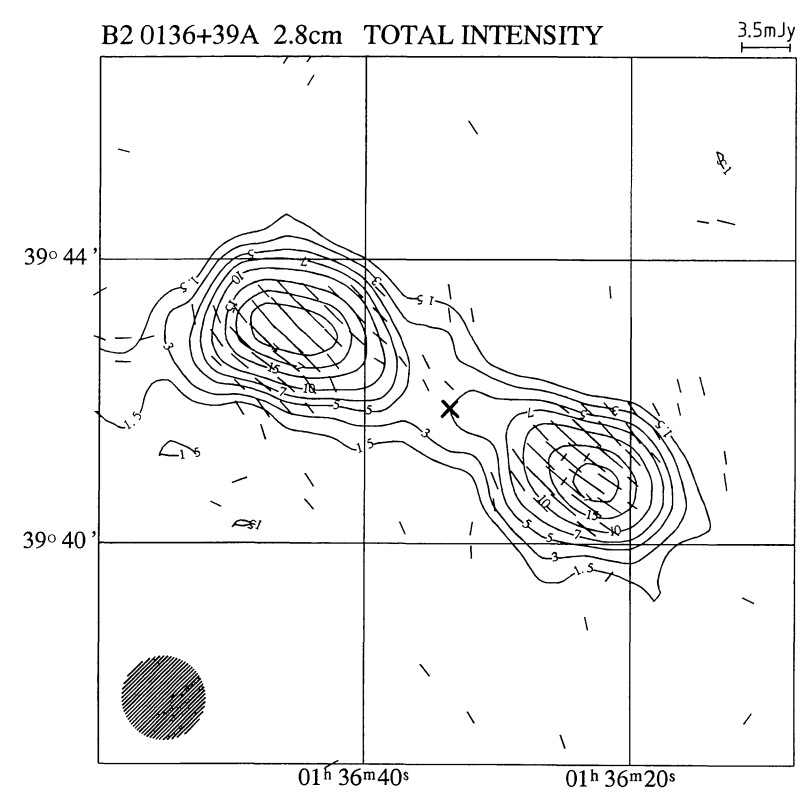


Fig. 1a.

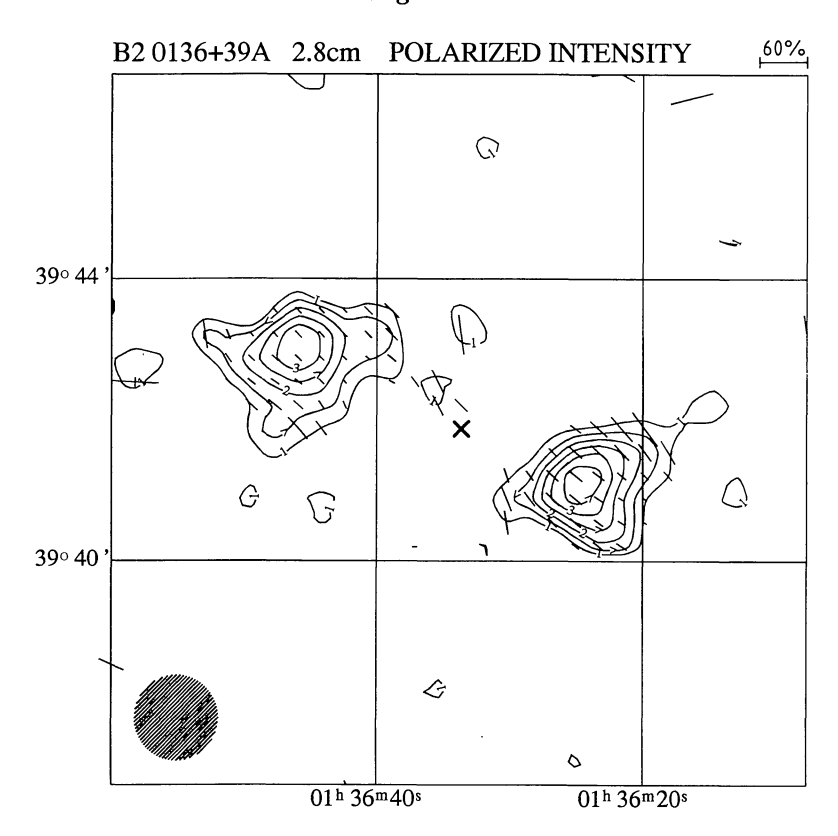


Fig. 1b.

Fig. 1 to 17. Maps of the B2 sources observed at 10.6 GHz. For each source, the contour map of the total intensity is shown in (a), with vectors representing the magnetic field orientation superimposed, with their lengths proportional to the polarized intensity. Contour maps of the polarized intensity are displayed in (b), with the lengths of the B-vectors proportional to the depolarization. Contour values are compiled in Table 2, the scales of the polarization vectors are indicated by the bar in the upper right, and the beam size by the hatched circle in the lower left of each map

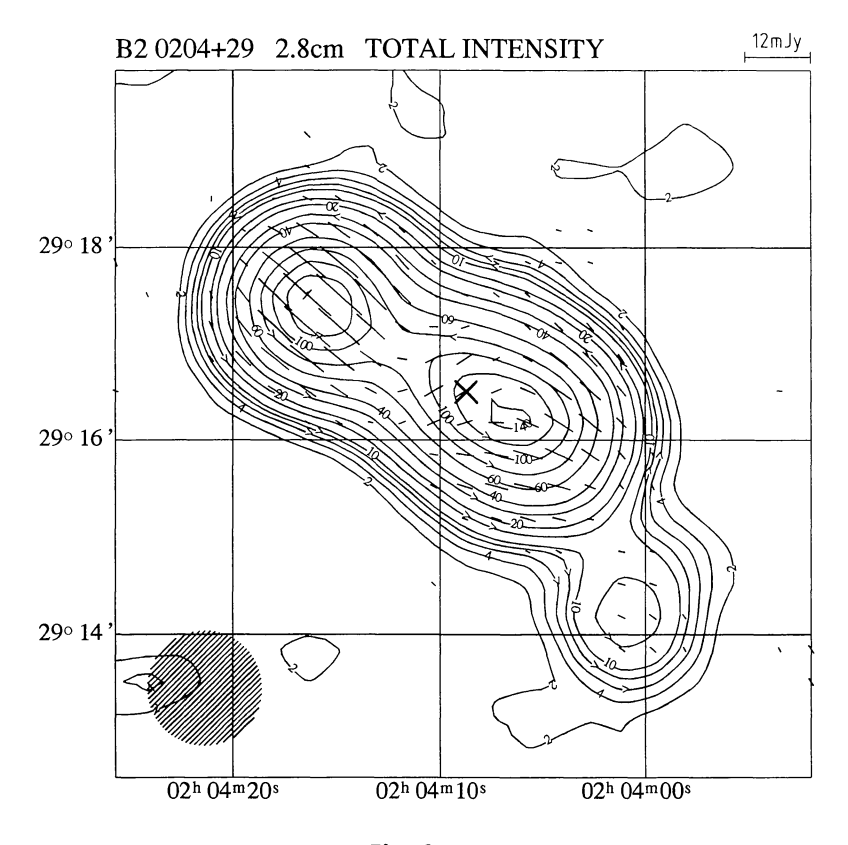


Fig. 2a.

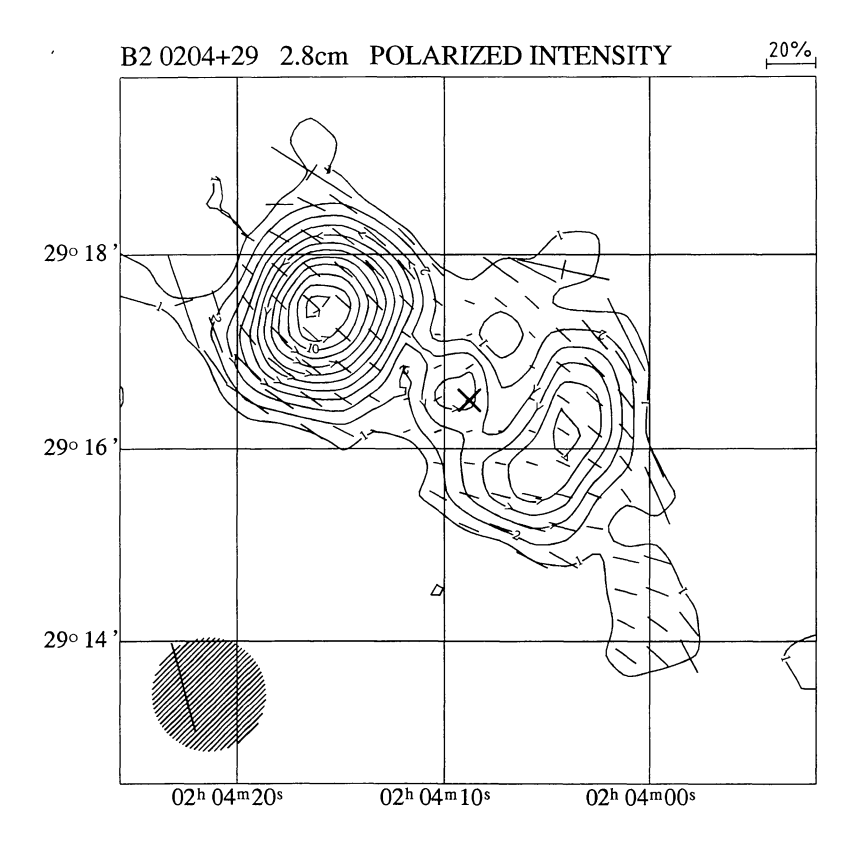


Fig. 2b.

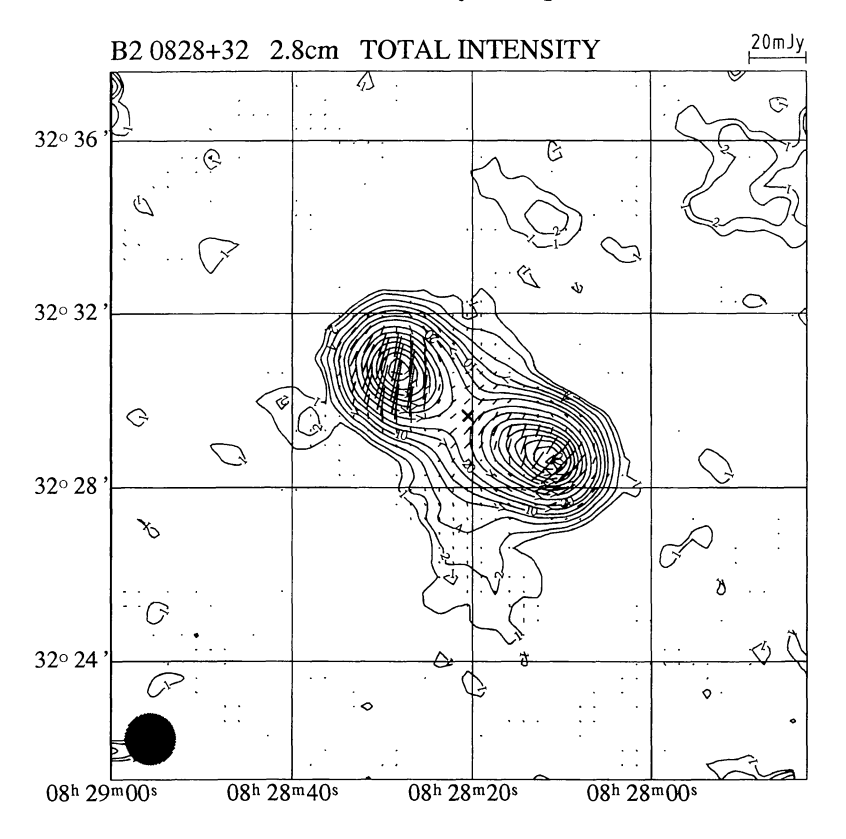


Fig. 3a.

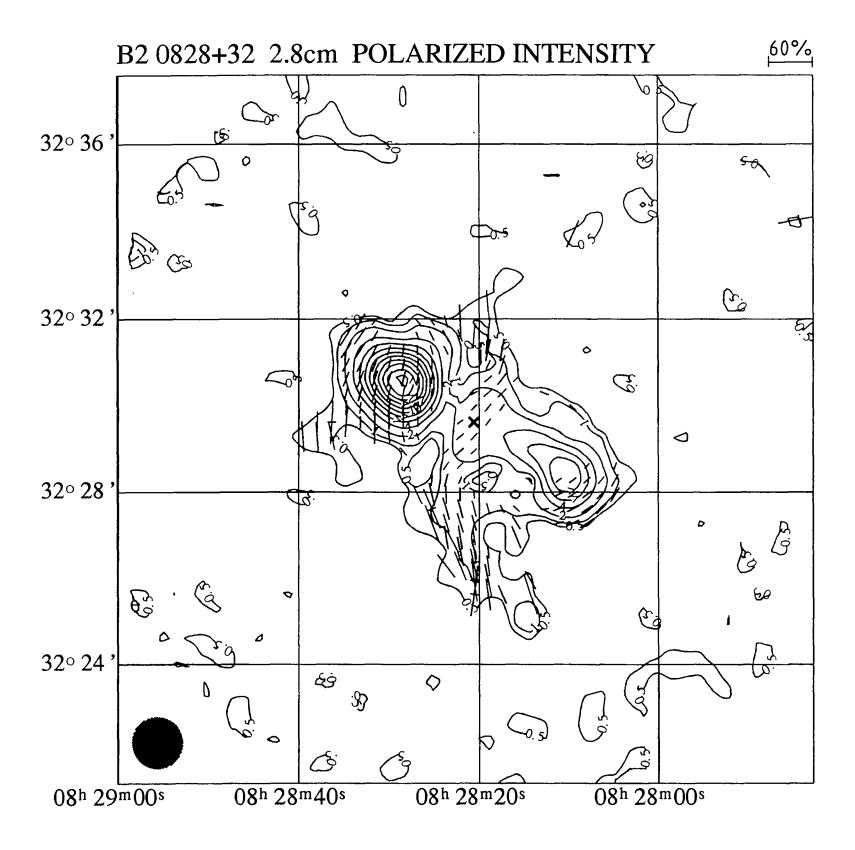


Fig. 3b.

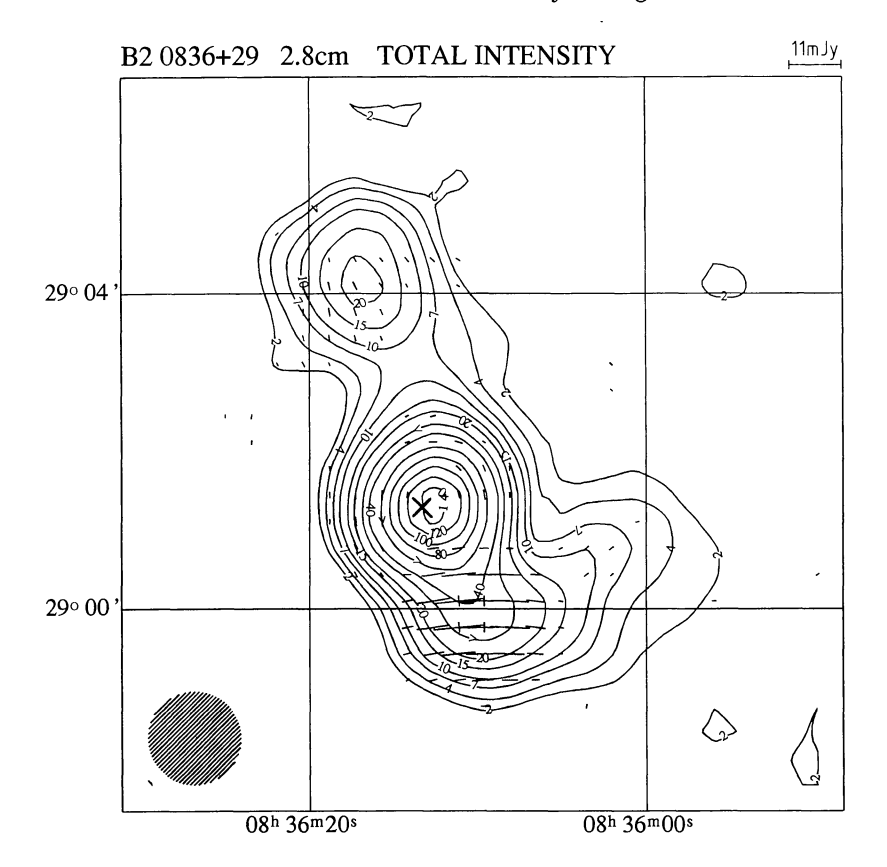


Fig. 4a.

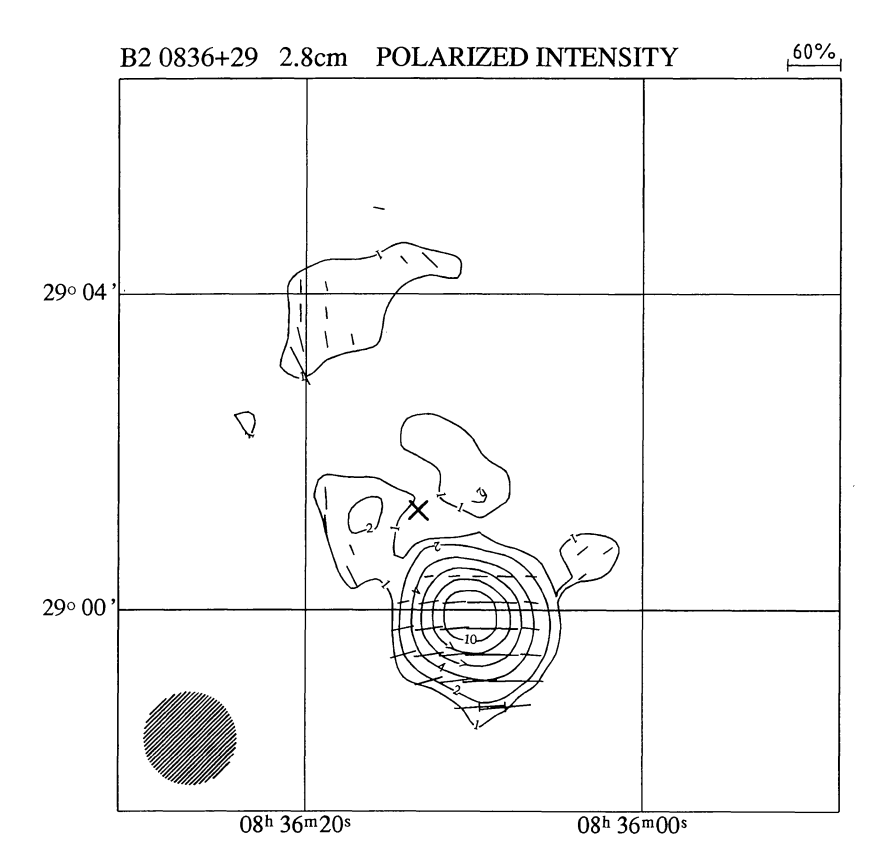


Fig. 4b.

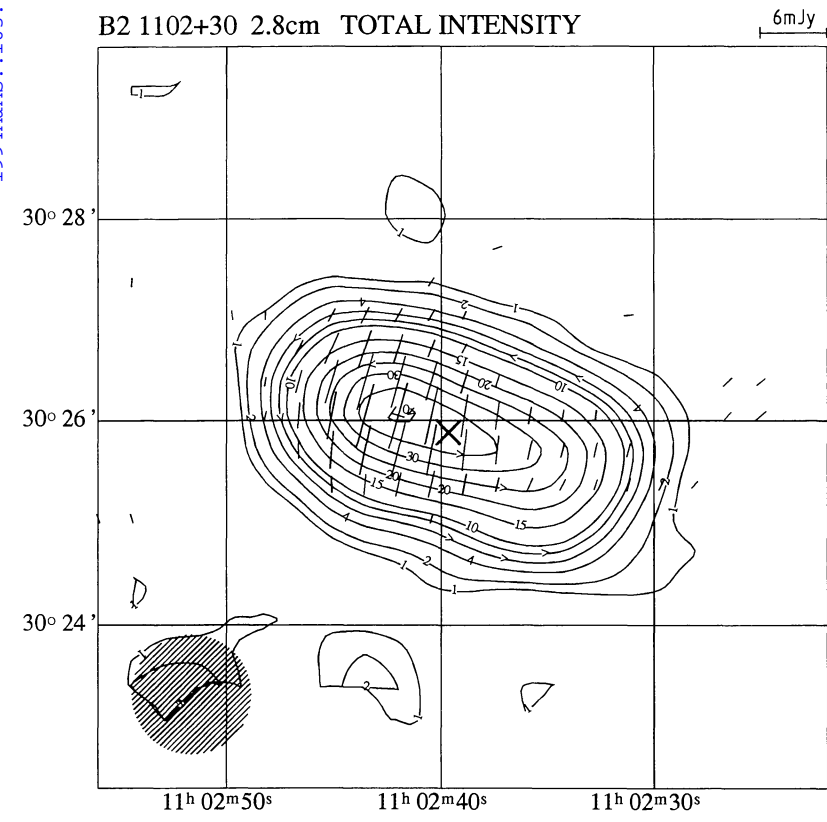
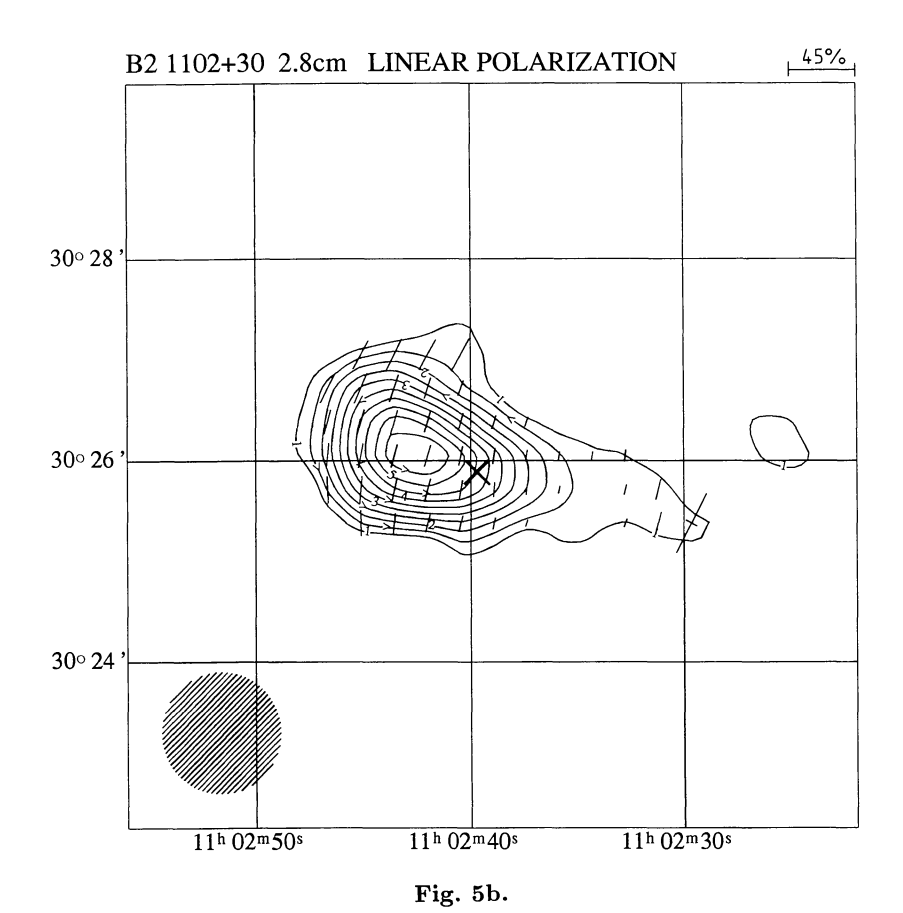


Fig. 5a.



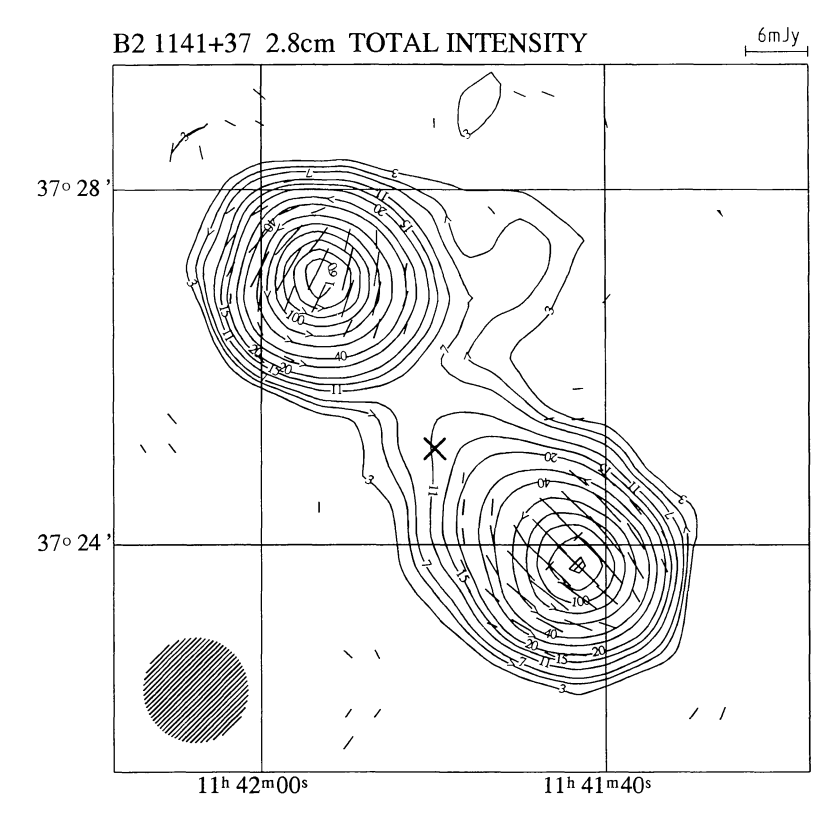


Fig. 6a.

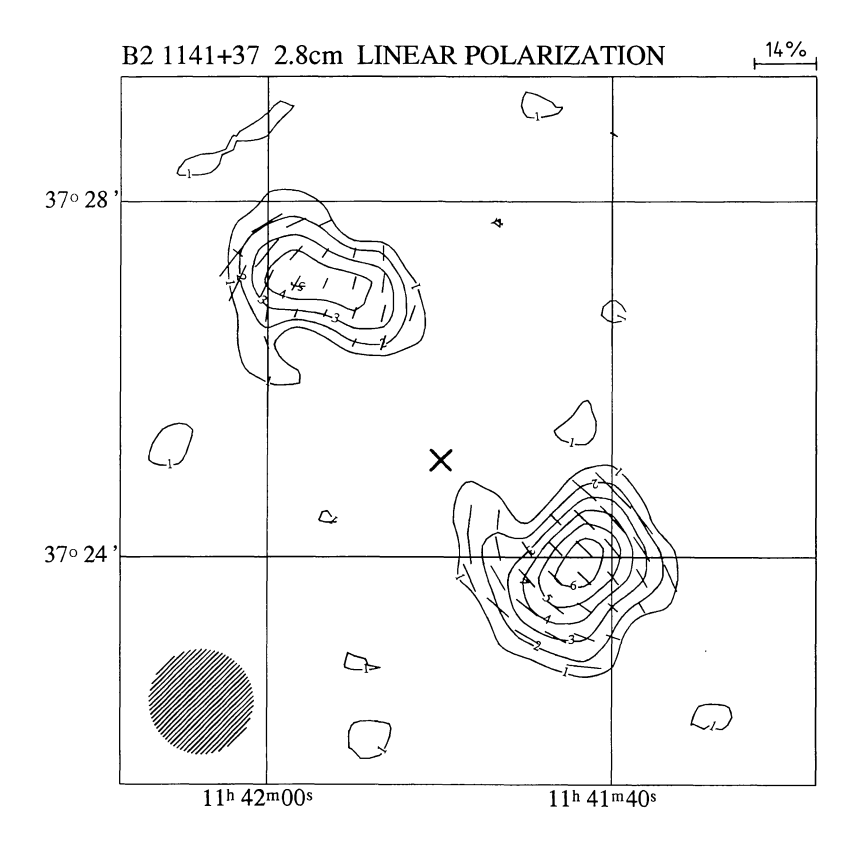


Fig. 6b.

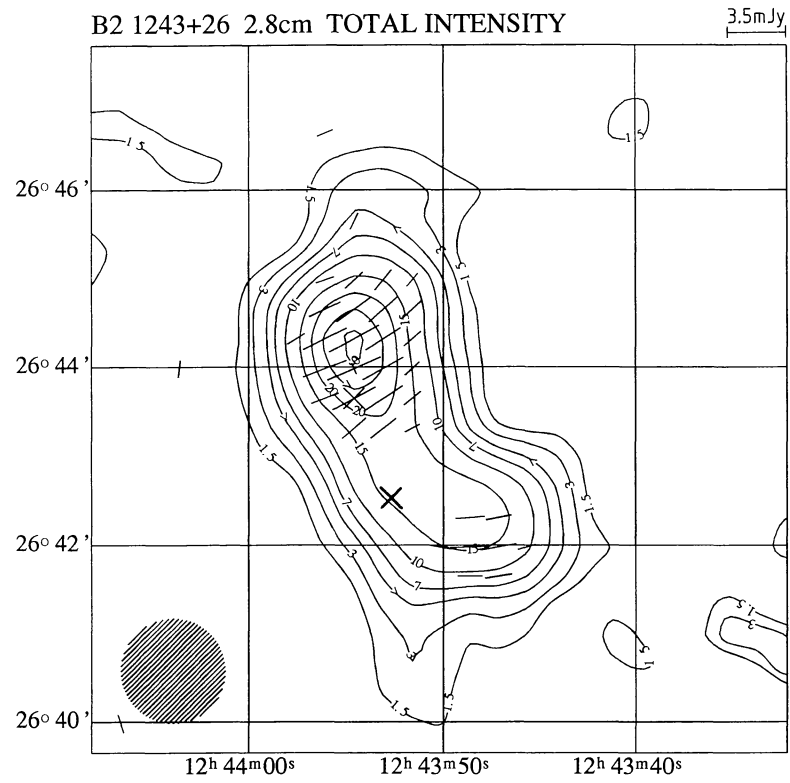


Fig. 7a.

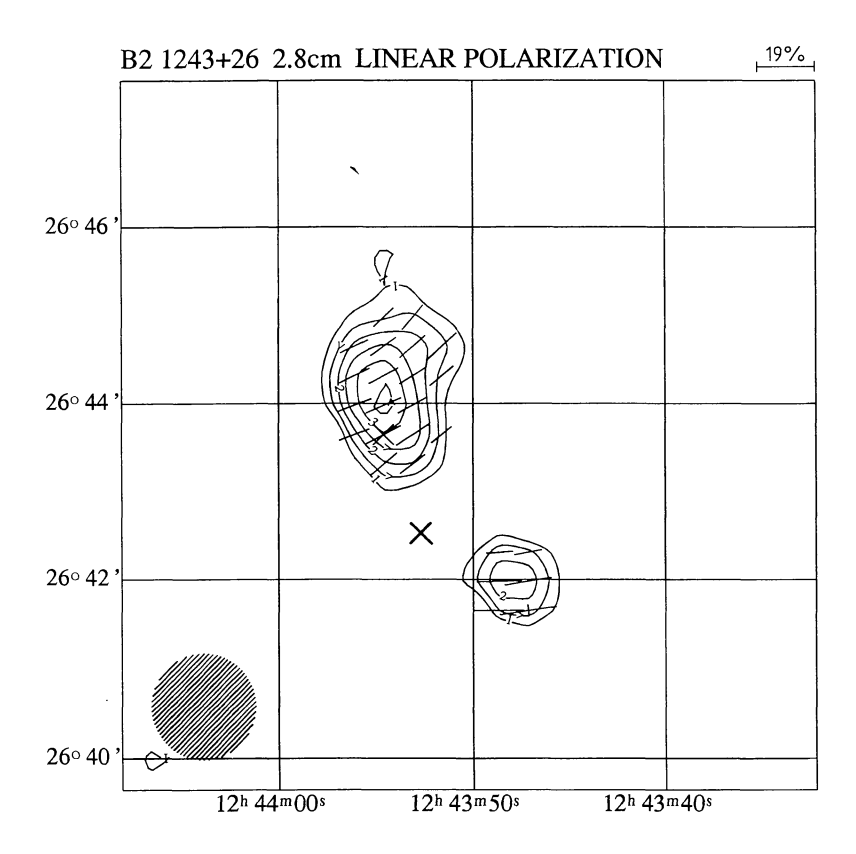


Fig. 7b.

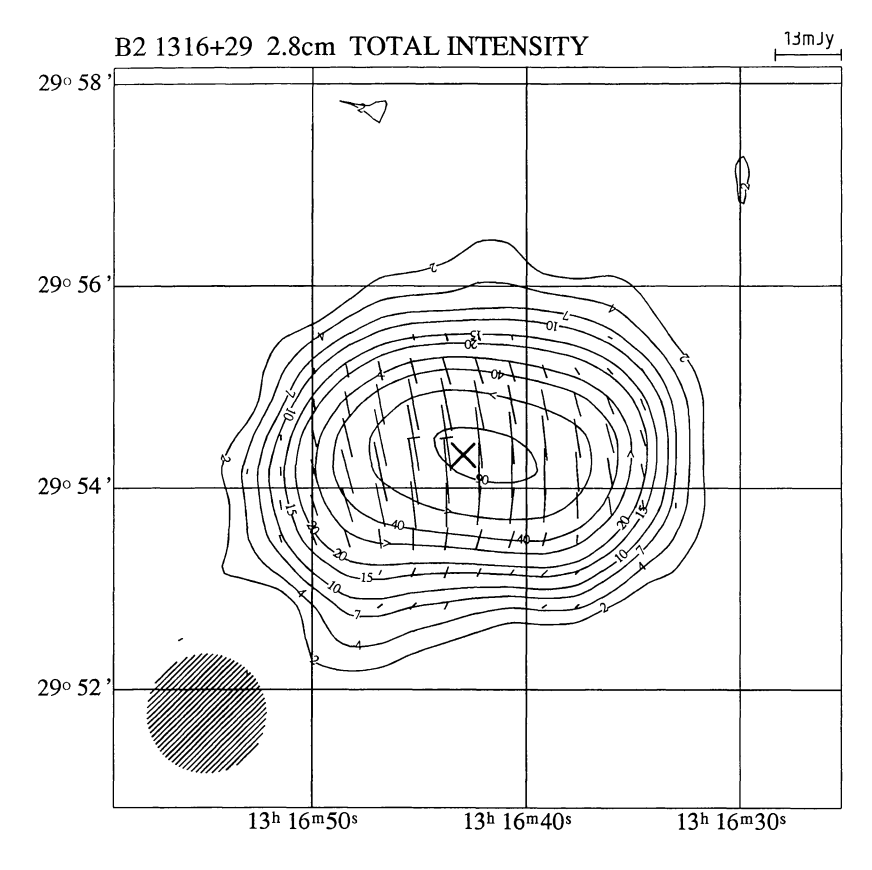


Fig. 8a.

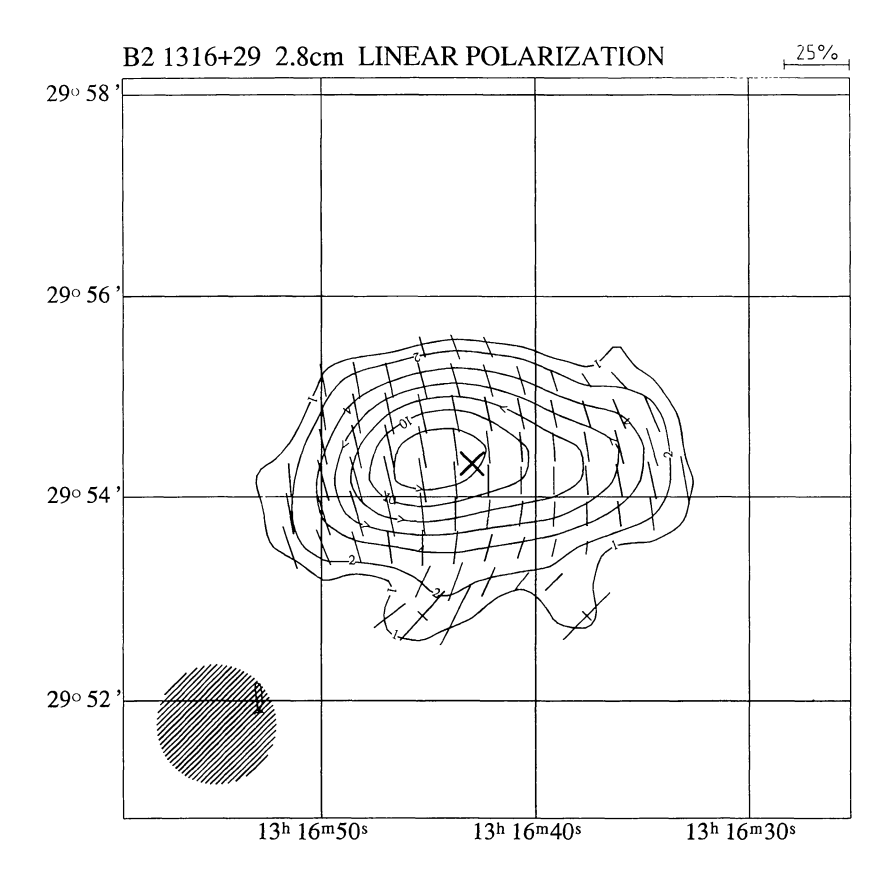


Fig. 8b.



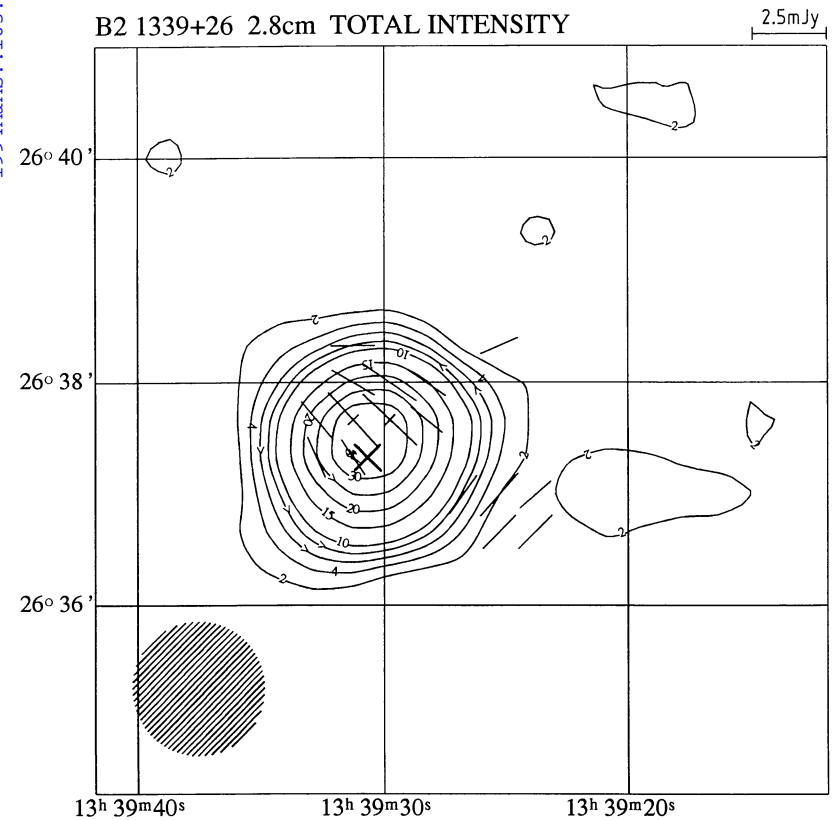


Fig. 9a.

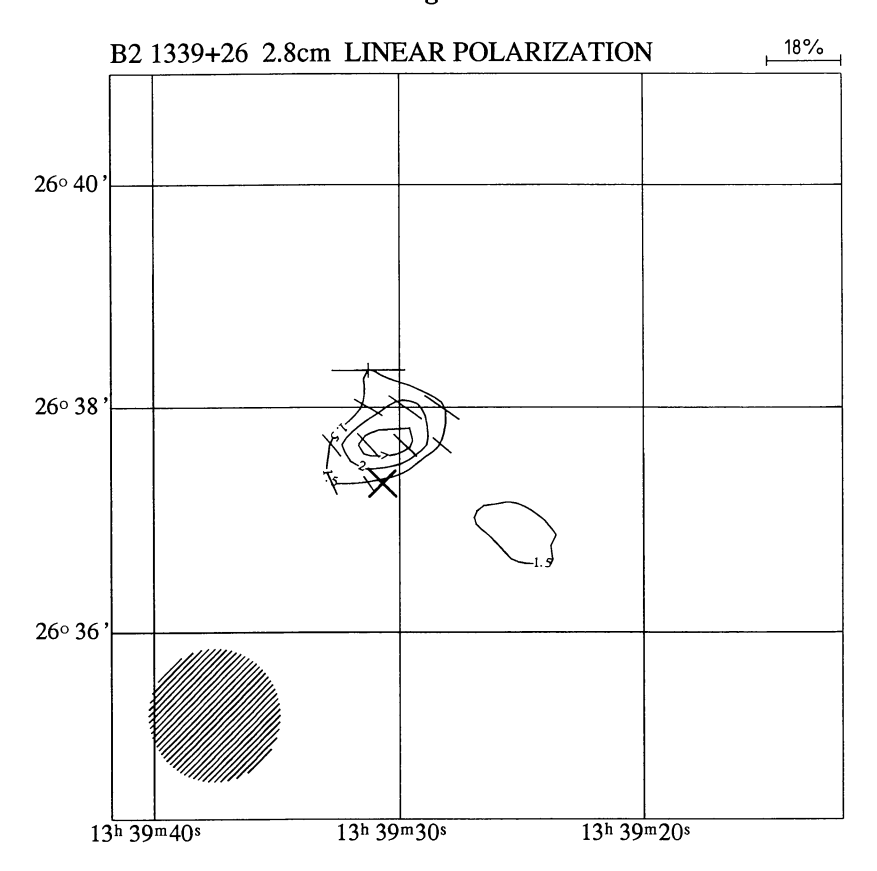


Fig. 9b.

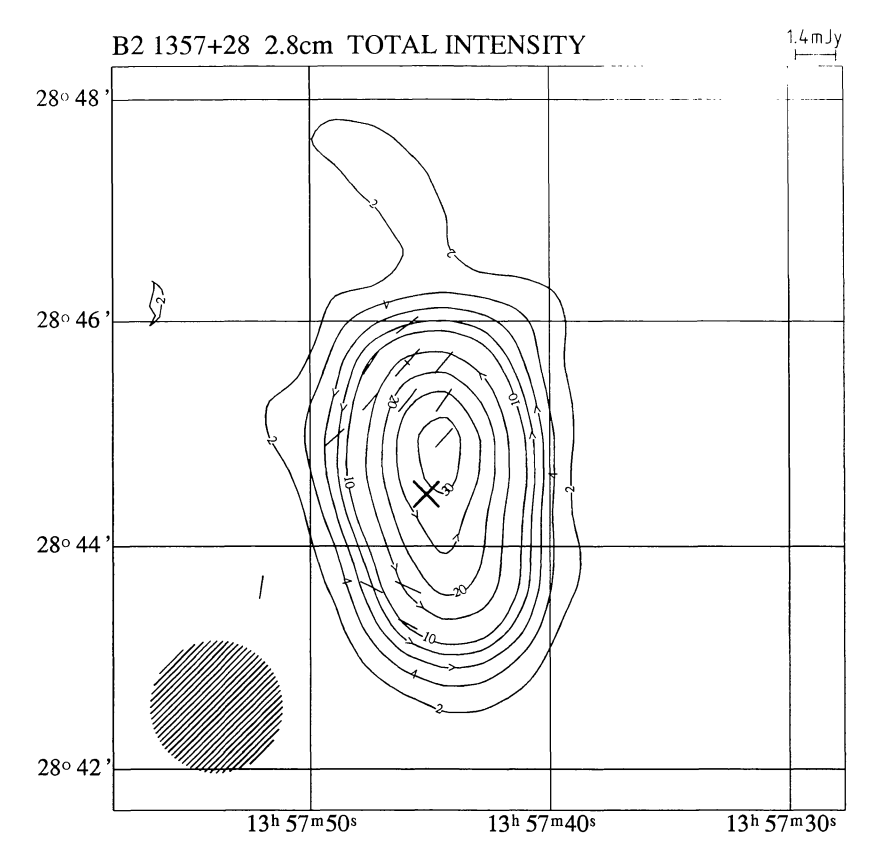


Fig. 10a.

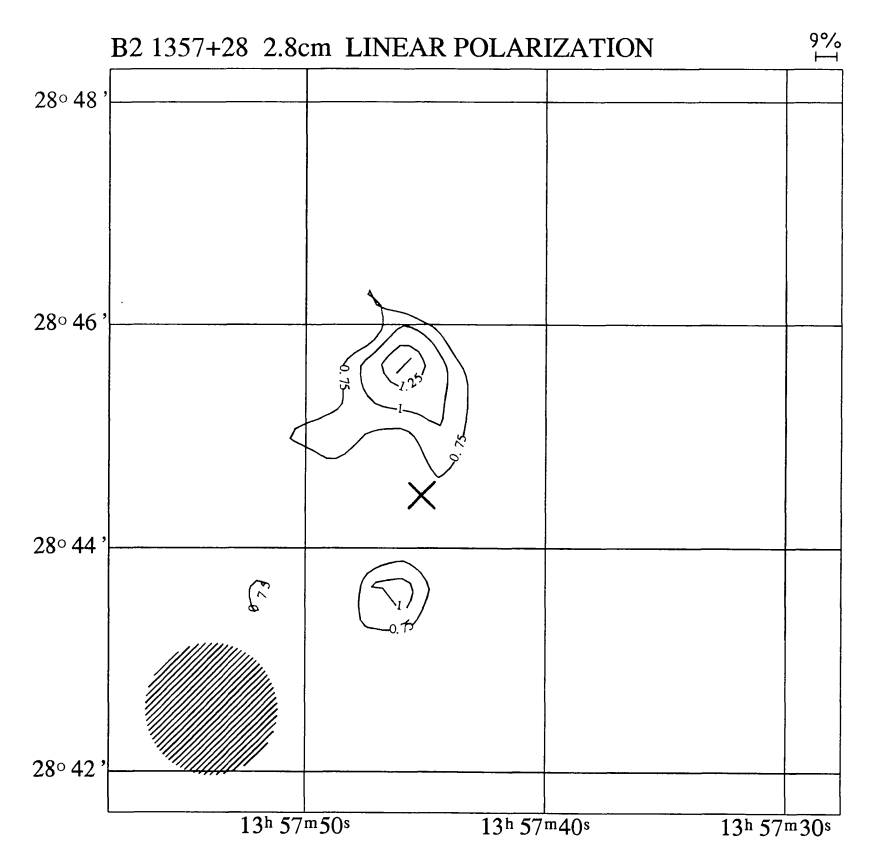


Fig. 10b.

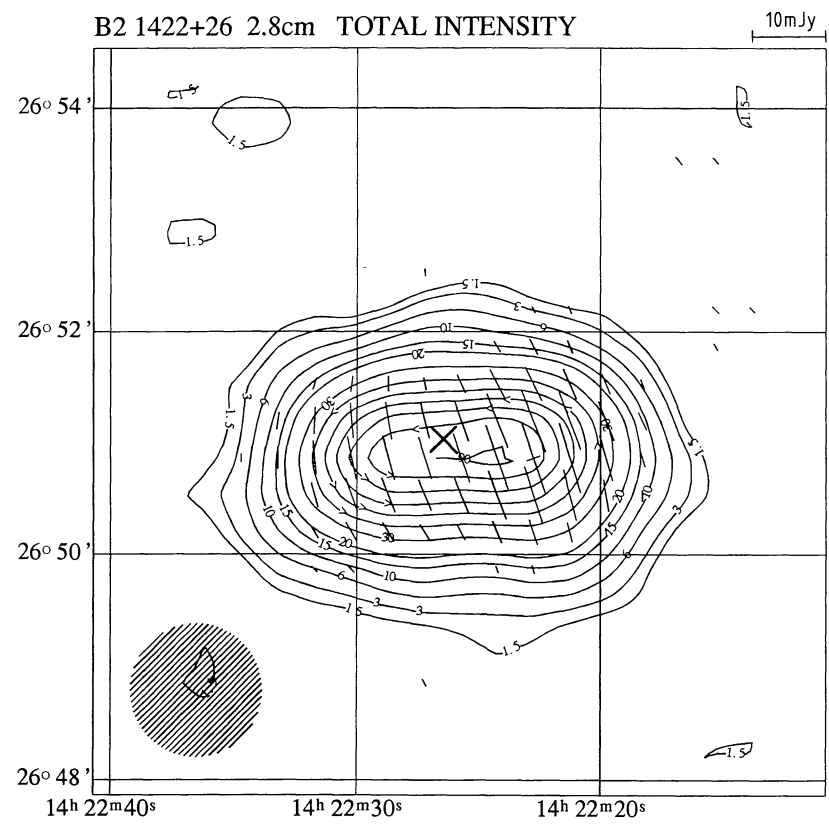


Fig. 11a.

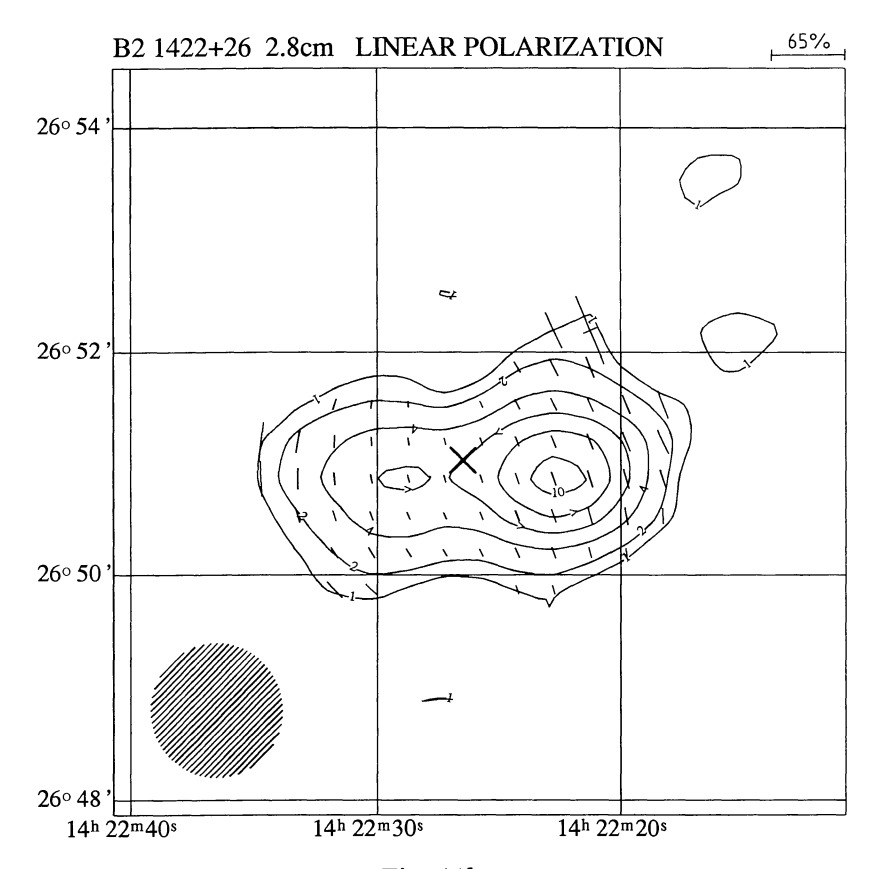
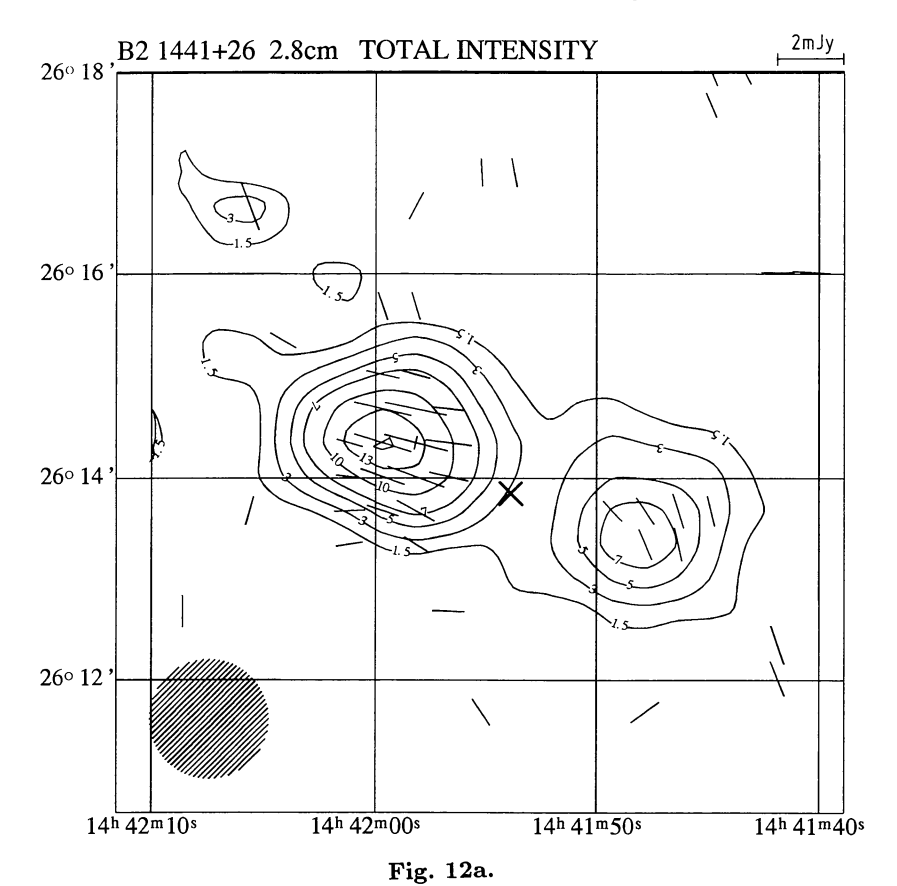
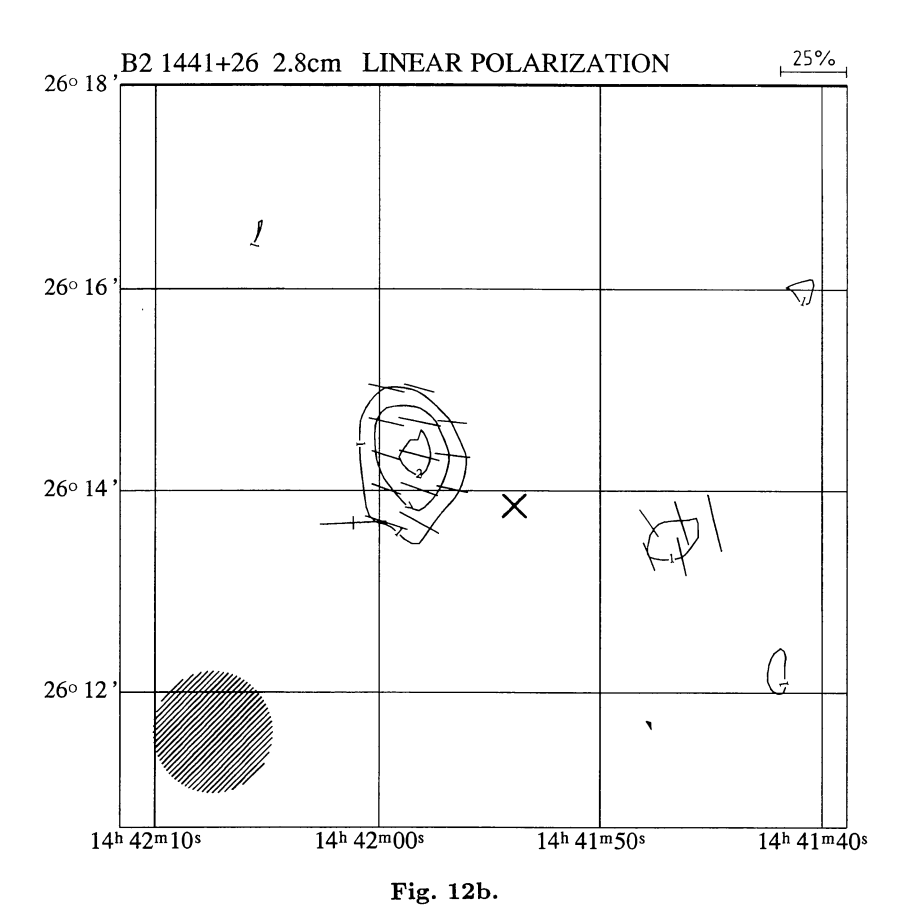


Fig. 11b.





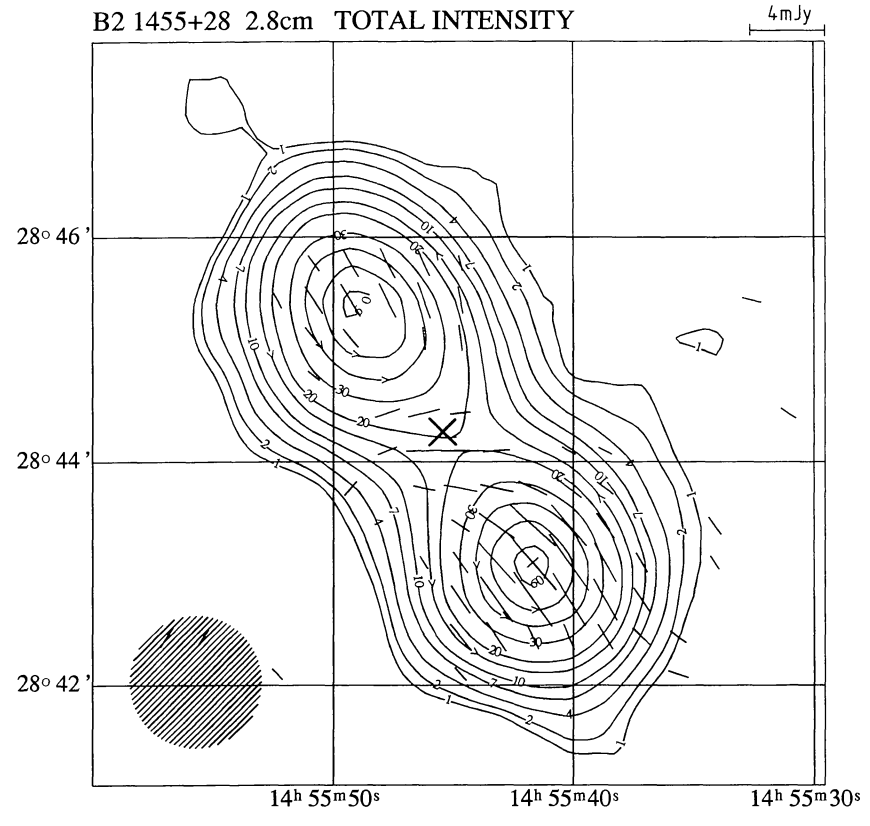


Fig. 13a.

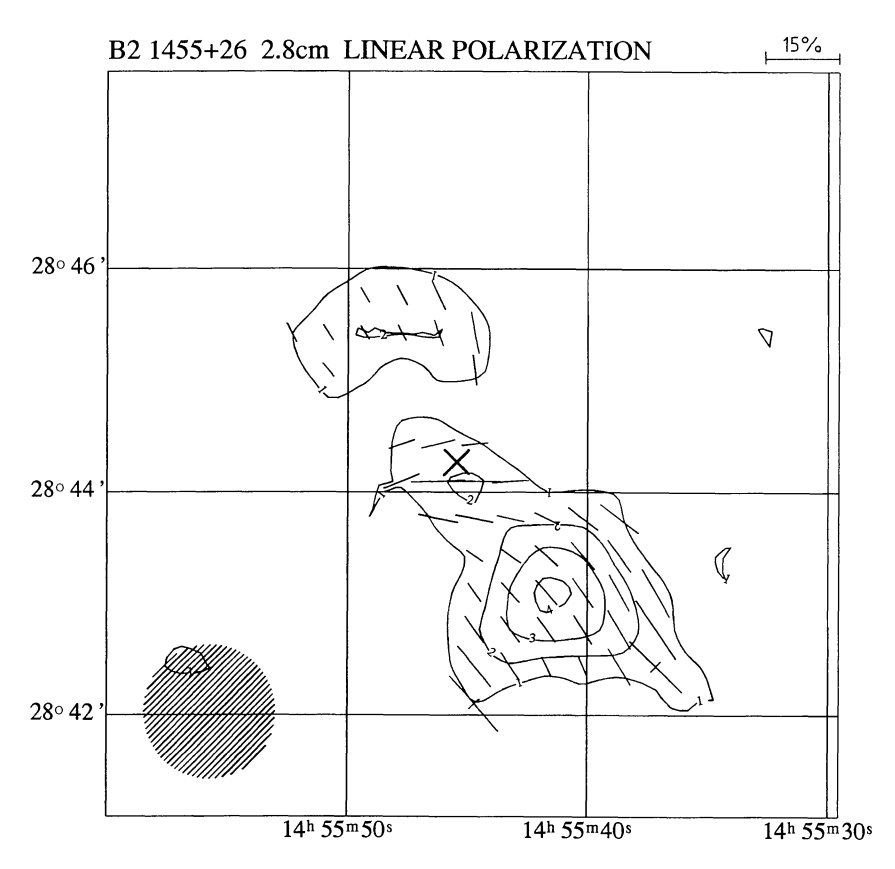


Fig. 13b.

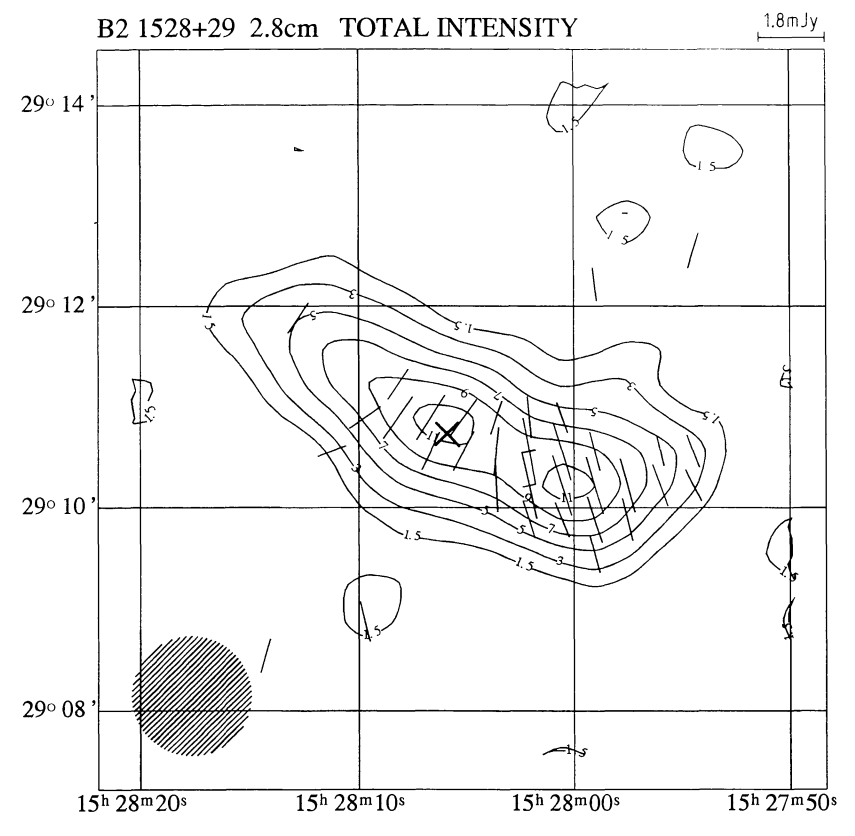


Fig. 14a.

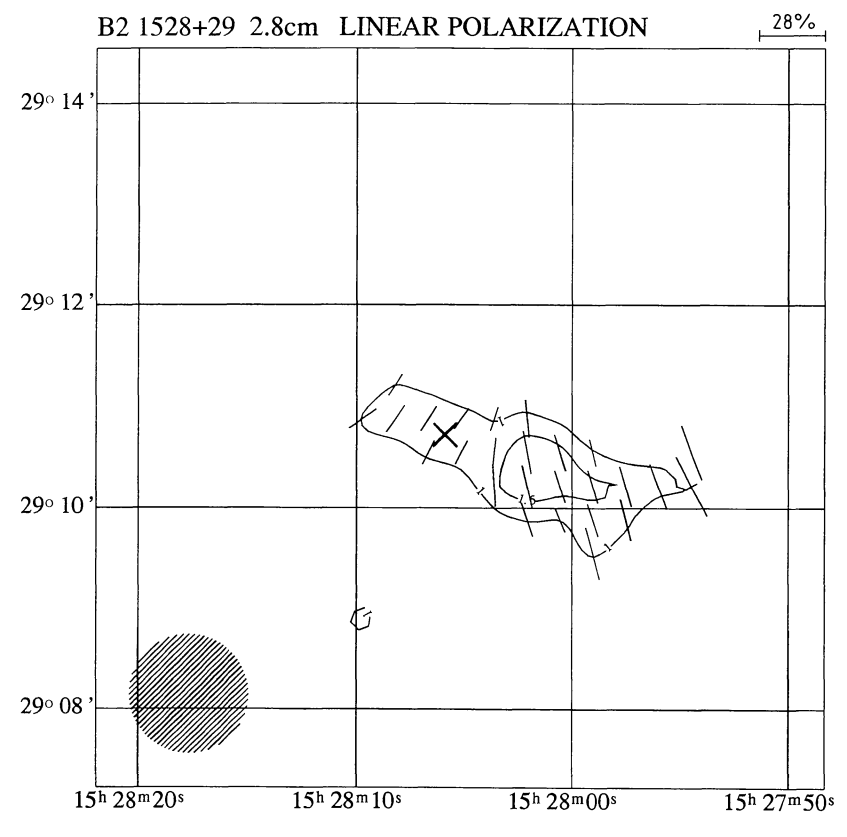
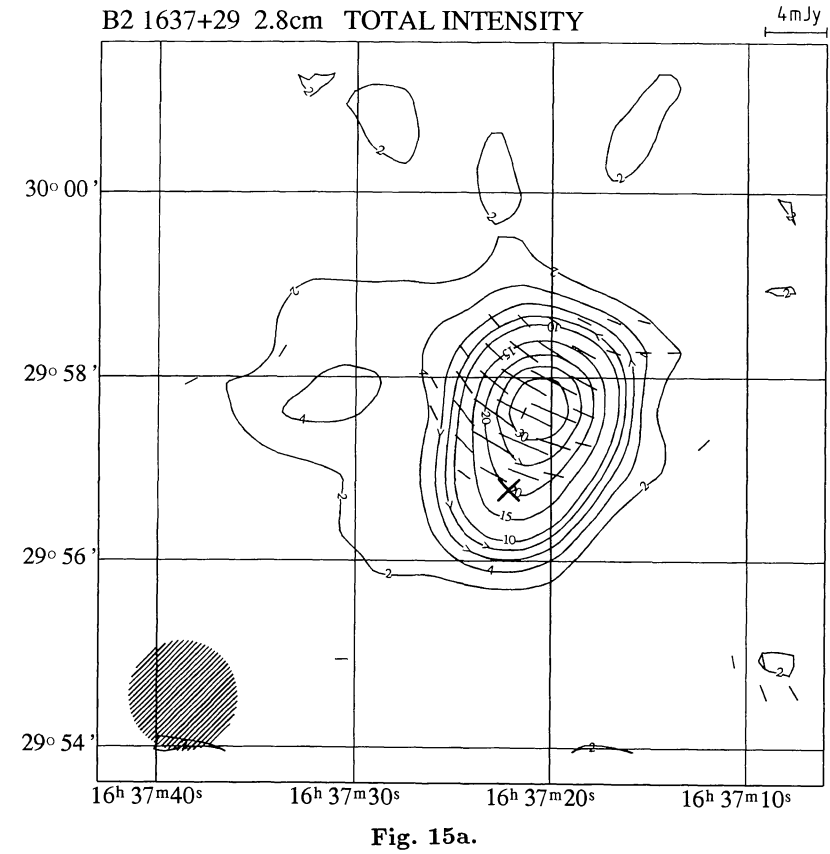
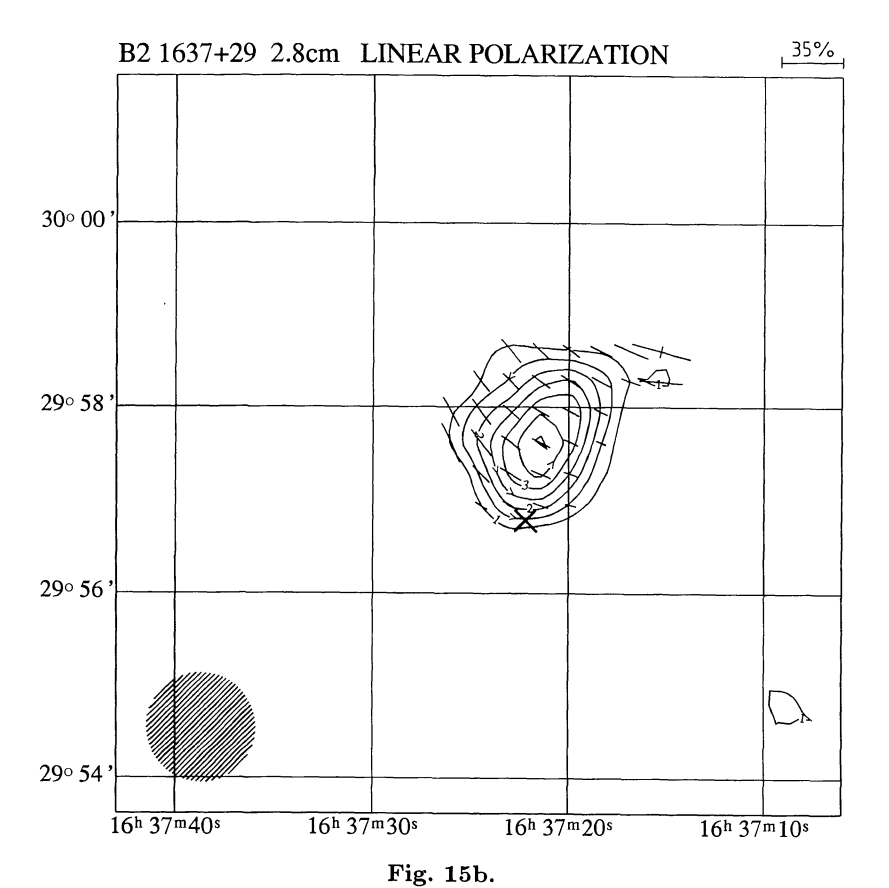


Fig. 14b.





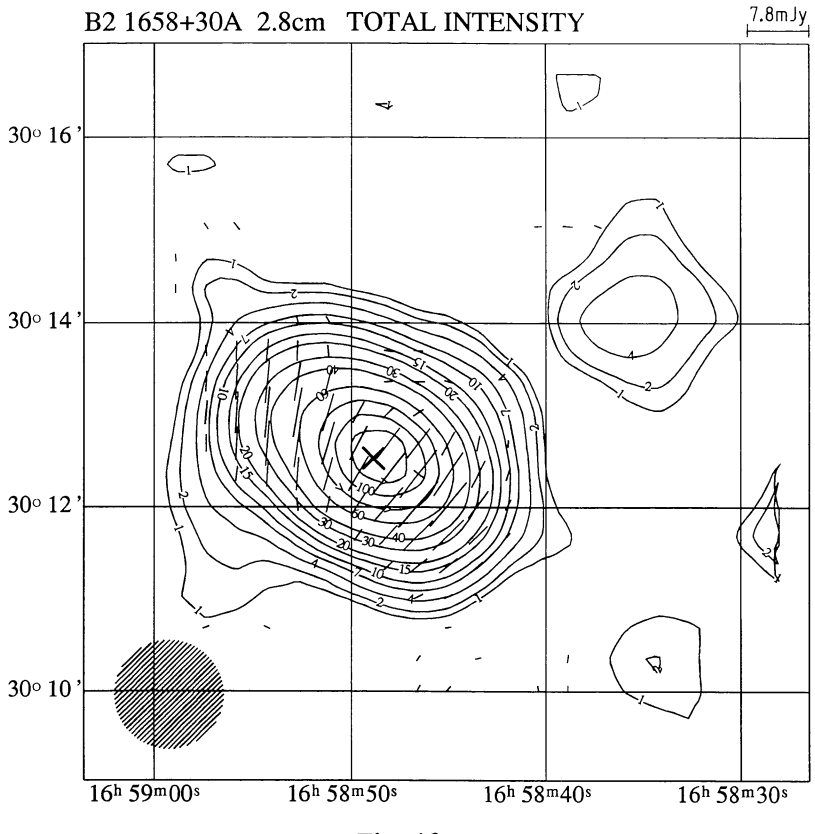


Fig. 16a.

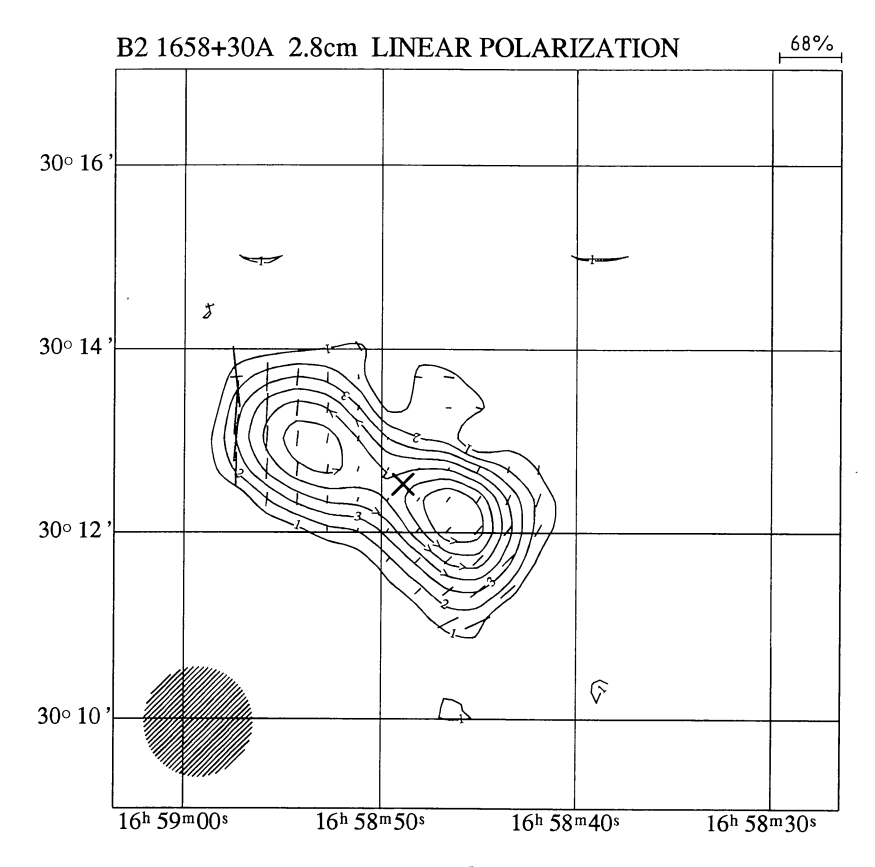


Fig. 16b.

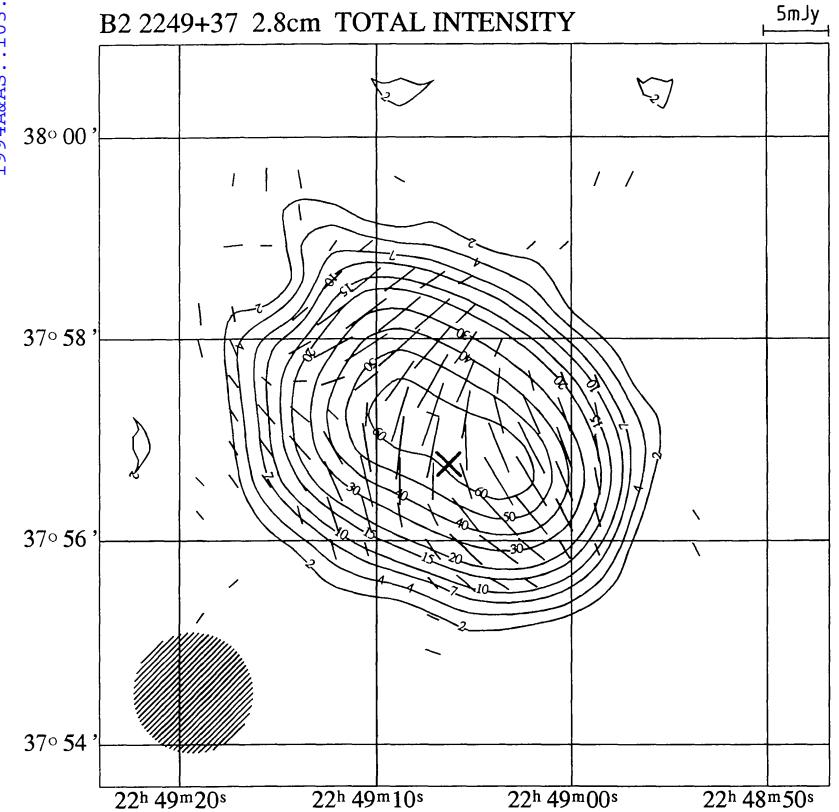


Fig. 17a.

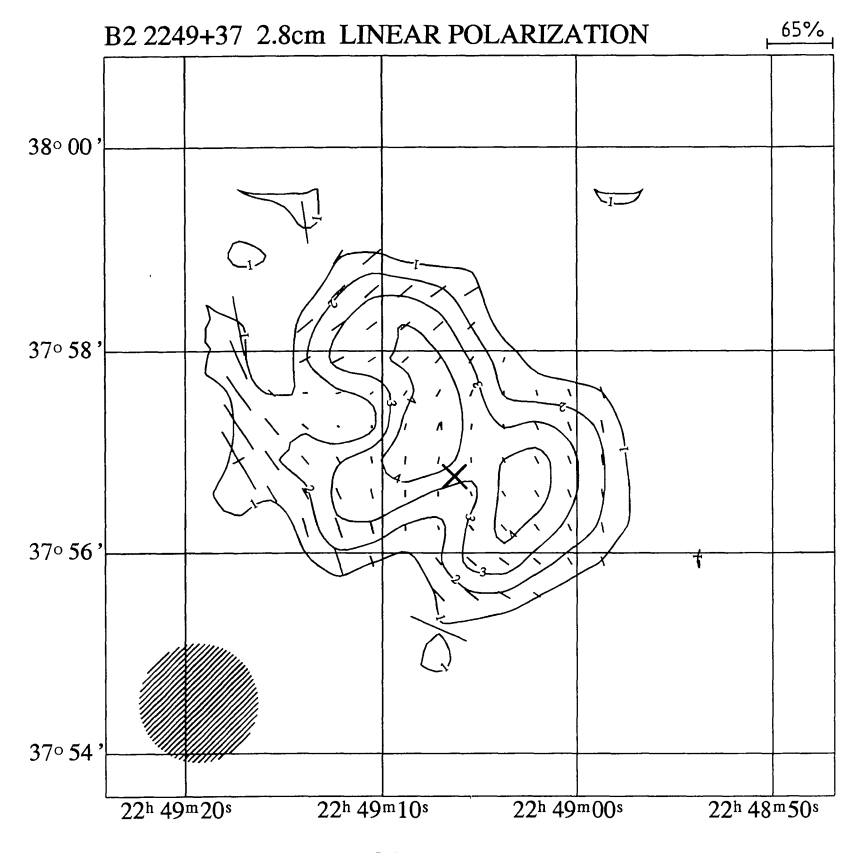
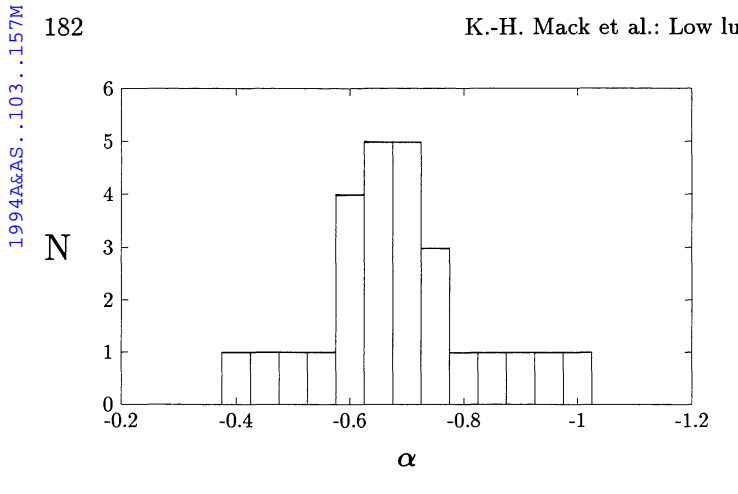


Fig. 17b.





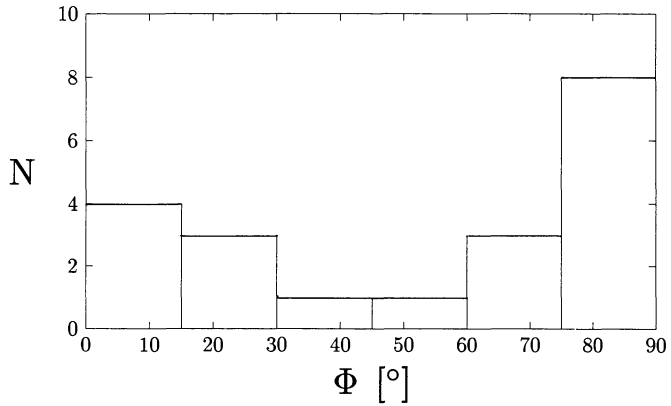


Fig. 18. Histogram of the integral source spectral indices derived between 408 MHz and 10.6 GHz

Fig. 20. Histogram of the relative orientations Φ of the mean magnetic fields with respect to the source/jet axes

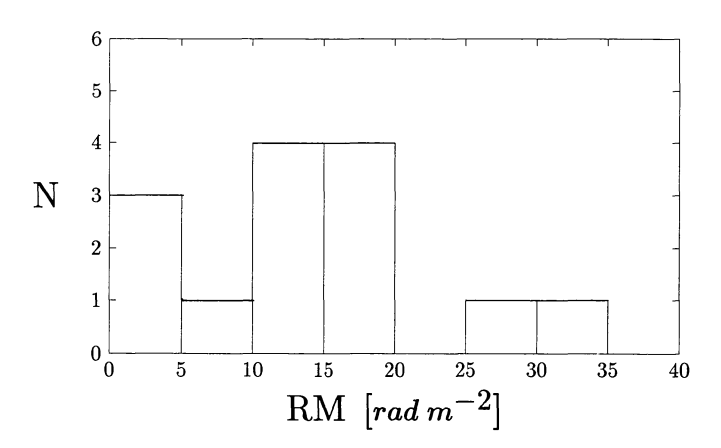


Fig. 19. Histogram of integral rotation measures of the sources